Article

Physical scaling predicts oil production rates and ultimate recovery from all horizontal wells in the Bakken shale

Wardana Saputra, Wissem Kirati and Tadeusz Patzek *

The Ali I. Al-Naimi Petroleum Engineering Research Center, King Abdullah University of Science and Technology, Thuwal 23955-6900, Saudi Arabia

* Correspondence: tadeusz.patzek@kaust.edu.sa

Version December 25, 2019 submitted to Preprints

Abstract: A recent study by the Wall Street Journal reveals that the hydrofractured horizontal wells in shales have been producing less than forecasted by the industry with the empirical hyperbolic decline curve analysis (DCA). As an alternative to DCA, we introduce a simple, fast and accurate method of estimating ultimate recovery (EUR) in oil shales. We adopt a physics-based scaling approach to analyze oil rates and ultimate recovery from 14,888 active horizontal oil wells in the Bakken shale. To predict EUR, we collapse production records from individual horizontal shale oil wells onto two segments of a master curve: (1) We find that cumulative oil production from 4,845 wells is still growing linearly with the square root of time; and (2) 6,401 wells are already in exponential decline after approximately seven years on production. In addition, 2,363 wells have discontinuous production records, because of refracturing or changes in downhole flowing pressure, and are matched with a linear combination of scaling curves superposed in time. The remaining 1,279 new wells with less than 12 months on production have too few production records to allow for robust matches. These wells are scaled with the slopes of other comparable wells in the square-root-of-time flow regime. In the end, we predict that total ultimate recovery from all existing horizontal wells in Bakken will be some 4.5 billion barrels of oil. We also find that wells completed in the Middle Bakken formation, in general, produce more oil than those completed in the Upper Three Forks formation. The newly completed longer wells with larger hydrofractures have higher initial production rates, but they decline faster and have EURs similar to the cheaper old wells. There is little correlation among EUR, lateral length, and the number and size of hydrofractures. Therefore, technology may not help much in boosting production of new wells completed in the poor immature areas along the edges of the Williston Basin. Operators and policy-makers may use our findings to optimize the possible futures of the Bakken shale and other plays. More importantly, petroleum industry may adopt our physics-based method as an alternative to the overly-optimistic hyperbolic DCA that yields an 'illusory picture' of shale oil resources.

Keywords: Scaling EUR; Unconventional; Refracturing; USGS; EIA

1. Introduction

In early 2019, seven major shale plays in the US produced nearly 70% of total US oil production. The Bakken shale is the second-largest oil producing play with the recent production rate of 1.45 million bbl of oil per day from 14,888 active horizontal hydrofractured wells. Therefore, it is important to have a reliable predictive model of oil production and ultimate recovery in the Bakken and other shale plays. In shale or tight oil reservoirs, where drainage area and communication between wells are limited [1,2], the estimated ultimate recovery (EUR) per well is the key indicator used to assess field-wide production potential. The most popular way of predicting EUR from a shale well is the traditional decline curve analysis (DCA) proposed by Arps 75 years ago. This method is favored by the industry, because it only requires production data to forecast future performance of each well and it is easy to implement for a large number of wells. Most published fieldwide predictions of EUR

 doi:10.20944/preprints201912.0334.v1

use DCA. Good examples are the Bakken predictions by the US Geological Survey [4,5] and US DOE Energy Information Administration [6].

In his seminal paper, Arps stated that DCA works by extrapolating oil rate observed in a pseudo-steady state (boundary-dominated) flow regime. Unfortunately, most shale wells do not reach pseudo-state flow regime during their entire existence, because of the vanishing matrix permeability. Thus, traditional DCA commonly overestimates EURs of shale wells [7,8]. In early 2019, the Wall Street Journal (WSJ) published an article entitled "*Fracking's Secret Problem–Oil Wells Aren't Producing as Much as Forecast*" [9,10]. The authors hired a third-party energy consulting firm to reforecast 16,000 wells operated by 29 top companies in the major shale oil basins in Texas and North Dakota, and then compared their new forecasts with the original corporate projections. The WSJ analysis revealed that two-thirds of the projections made by fracking companies appeared to be overly optimistic. Thousands of shale wells drilled between 2014 and 2017 are pumping on average 10% less oil and gas than their owners' forecasts. In certain regions, the discrepancy between forecasts and actual production is more than 50%. The total deficit is equivalent to one billion barrels of oil and gas that will *not* be produced over 30 years or to $30 billion at current oil price.

There are several new empirical methods that serve as alternatives to the industry-standard hyperbolic DCA, which is demonstrably optimistic in forecasting oil and gas production from shales. Ilk *et al.* (2008) proposed an empirical exponential rate decline model that matches production data better than the hyperbolic DCA in shale gas applications. Valko (2009) presented another form of the exponential rate decline analysis of hydrofractured gas wells in the Barnett shale. In (2010), Valko and Lee proposed the stretched exponential decline curve. Duong (2011) introduced an empirical model in which the ratio of rate to cumulative production follows a straight line on a log-log plot vs time, and used this model to fit oil and gas production in the Bakken and Barnett. Clark *et al.* (2011) developed a logistic growth model for production forecasting in shales and implemented it for the Bakken shale. Gong *et al.* (2014) incorporated uncertainties into the production forecasts of the Barnett shale and introduced a Bayesian probabilistic DCA. Paryani *et al.* (2017) proposed a similar probabilistic DCA that simplifies the Bayesian inference and applied it to more Barnett wells. Zhang *et al.* (2016) formulated the Extended Hyperbolic DCA to improve production data fitting in shales.

Empirical models are simple, but they also are mere curve fits, whose parameters have little physical meaning and cannot be generalized. In hyperbolic DCA, for example, the exponent b is adjusted to fit production data, notwithstanding several studies that have tried to elucidate its physical meanings [19–21]. Another limitation of most empirical models is their inability to capture the two regimes of oil and gas production in shales that are transient-linear flow at early times and boundary-dominated flow at later times on production [22]. We posit that a physics based analytic or numeric solution is more predictive than an empirical decline curve. Unfortunately, many analytical solutions proposed in recent years remain unpopular, because of the high amount of data required and complexity of these solutions. Aybar *et al.* (2014) and Aybar *et al.* (2015) proposed the rather involved semi-analytical and numerical predictions of performance of shale gas wells; their solutions were a step in the right direction.

In this paper, we reintroduce our physics-based scaling approach that is based on an analytical solution of transient oil flow. The physical scaling approach was originally developed to predict gas production in the Barnett shale [25,26]. In 2017, we extended our earlier gas production scaling to predict EURs from thousands of oil wells in the Eagle Ford [27]. In this paper, in turn, we extend the Eagle Ford scaling to predict EURs from the 14,888 existing horizontal, hydrofractured black oil wells in the Bakken. We consider the simplest model of oil production consistent with the first order physics and idealized geometry of the extraction process. In principle, the solution of this model depends on many parameters, but in practice – for a given shale play –, all but two can be fixed at a field region-average values, resulting in an exact solution of a nonlinear transient pressure diffusion problem with the simplified geometry of the hydrofractured horizontal wells as the boundary condition. At early times, the scaled oil production rate declines as one over the square root of dimensionless

Preprints (www.preprints.org) | NOT PEER-REVIEWED | Posted: 25 December 2019 doi:10.20944/preprints201912.0334.v1

time on production, reflecting transient oil flow. Later, oil production rate declines exponentially indicating boundary-dominated flow. In addition, we combine the physical scaling approach with time superposition to resolve erratic production records of the refractured old Bakken wells, and of the wells that were put on artificial lift with time-varying downhole conditions.

To predict EURs, we collapse production records from individual horizontal oil wells onto two different segments of an almost universal scaling curve. The scaling is performed by adjusting two parameters, the pressure interference time, τ, and the initial mass of oil in the SRV, $\mathcal{M}$. Our scaling is described in section 3.1.1 and section 3.1.2. The scaling is easy to program and works perfectly for large production data sets. Even though our approach is mechanistic, it preserves the simplicity of traditional DCA by relying only on average reservoir rock and fluid properties and on well-by-well time series of oil production. In a slightly different context, our physical scaling approach has been proven to have the same predictive power as full reservoir simulation, while being several orders of magnitude faster [28]. The EURs calculated from the physical scaling are compared with the latest published results by EIA.

We map water cuts, gas oil ratios, and calculated EURs of Bakken wells to locate the best producing region in the Williston basin. We also analyze how recent advancements of well completion technologies influence EUR. Operators and policy-makers may use our findings to guide sensible development of the Bakken and other shale plays. More importantly, petroleum industry may adopt our simple, fast and accurate method to predict oil production in shales as an alternative to the overly-optimistic hyperbolic DCA that yields an 'illusory picture' of shale oil resources [9].

2. Overview of the Bakken Shale Play

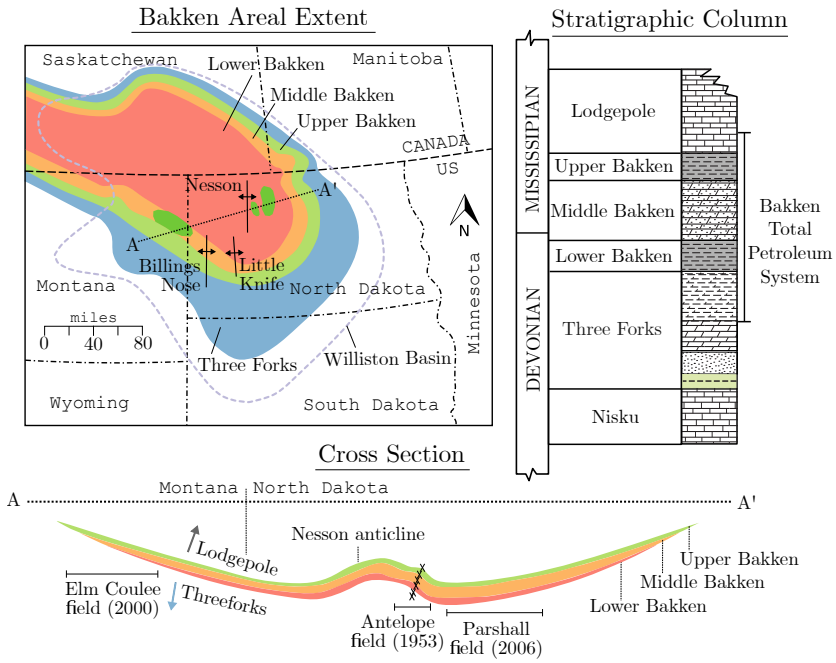

Figure 1. Areal extent, stratigraphic column, and cross section of the Bakken Total Petroleum System (TPS), modified from [4,29,30].

The Bakken mudrock play was discovered in 1953, in the Antelope Field, North Dakota, with the completion of the #1 Woodrow Starr by Stanolind Oil and Gas Corporation [31]. Outside of Antelope field, the Bakken formation was not considered to be economically viable because it was generally impermeable [31,32]. The success of old vertical wells drilled in the Antelope Field depended upon natural fracture networks in the Bakken and Three Forks (Sanish) Formations [32].

Preprints (www.preprints.org) | NOT PEER-REVIEWED | Posted: 25 December 2019 doi:10.20944/preprints201912.0334.v1

The Bakken was not developed until the early 2000s, when about 20,000 barrels of oil per day were produced from the Elm Coulee field in Montana. Improvements of horizontal drilling techniques and advancements in hydraulic fracturing enabled massive drilling in the Bakken in the past ten years. By 2014, more than 10,000 horizontal wells were drilled in 14 counties in Montana and North Dakota, leading to the first production peak in the Bakken at 1.22 Mbopd. In early 2019, Bakken ranked as the second-largest oil producer in the U.S., with the second major oil peak of 1.45 Mbopd from 14,888 horizontal, hydrofractured oil wells. The predicted technically recoverable oil in the Bakken region is about 7.38 billion barrels of oil according to the US Geological Survey [4], and 15.6 billion barrels of oil according to the US DOE Energy Information Administration [6].

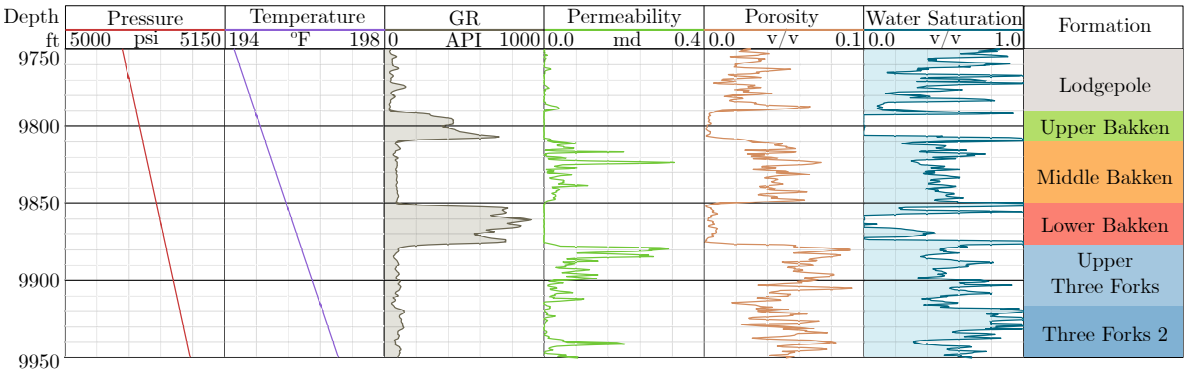

(a) Well - 33-055-XXXXX

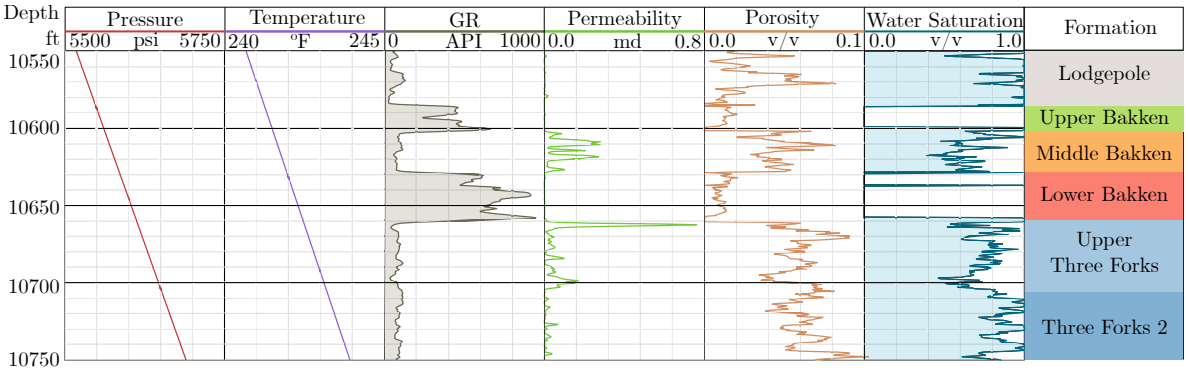

(b) Well - 33-053-XXXXX

Figure 2. Bakken well log data from the North Dakota Department of Mineral Resources - Oil and Gas Division home page.

The areal extent, cross-section, and the stratigraphic column in the Bakken are shown in Figure 1. The Bakken total petroleum system (TPS) lies on a bowl-like intracratonic Williston Basin, which covers an area of 200,000 square miles (518,000 km^2) across parts of North Dakota and Montana in the US, and into the Saskatchewan Province in Canada. The Bakken TPS is a continuous petroleum system that consists of three Bakken members, the Upper Three Forks and the Lower Lodgepole [4]. The Upper Bakken and the Lower Bakken are world class shale formations with total organic carbon (TOC) of about 10%. These formations are the source of hydrocarbons in the dolomitic Upper Three Forks and silty dolomitic Middle Bakken members. The Middle Bakken and Upper Three Forks formations are the two major drilling targets for recent field developments.

The average reservoir properties of the three Bakken members and the Upper Three Forks were derived from well log data in McKenzie and McLean counties, North Dakota, (Figure 2), and are summarized in Table 1.

Preprints (www.preprints.org) | NOT PEER-REVIEWED | Posted: 25 December 2019 doi:10.20944/preprints201912.0334.v1

Table 1. The average reservoir properties from well log data shown in Figure 2

Formation	Upper Bakken	Middle Bakken	Lower Bakken	Upper Three Forks
Depth (ft)	10,197	10,223	10,254	10,289
Pressure (psia)	5,325	5,338	5,355	5,373
Temperature (°C)	218	218	219	219
Gamma Ray (°API)	431	83	690	81
Permeability (mD)	1.4×10^{-4}	4.5×10^{-2}	2.0×10^{-4}	4.7×10^{-2}
Porosity	0.008	0.046	0.008	0.058
Water Saturation	0.20	0.57	0.22	0.65
Thickness (ft)	19	33	30	40

The average formation depth of all layers is about 10,000 ft (3,048 m). At this depth, the initial formation pressure and temperature are about 5,300 psia (37 Mpa) and 220°F (105°C), respectively. Because the Upper and Lower Bakken formations are shales, the gamma-ray log readings there are as high as 690 °API and the permeability is as low as 200 nanodarcy (2×10^{-19} m^2). The main drilling targets, Middle Bakken and Upper Three Forks, have a better permeability of about 45 microdarcy (5×10^{-17} m^2). The Upper Three Forks formation has a slightly higher porosity and thickness than those in the Middle Bakken, but it also has a higher water saturation, indicating that the Three Forks wells must produce more water.

USGS [4] divided the huge Bakken area into five assessment units (AUs) based on maturity levels, basin structures, and petrophysical properties. These five assessment units are Central Basin, Eastern Transitional, Elm Coulee-Billings Nose, Nesson-Little Knife, and Northwest Transitional. Figure 3 shows the surface locations of the 14,888 horizontal oil wells in the Bakken colored by the AUs. These AUs were delineated using geology and statistics for the continuous accumulation of hydrocarbon in the Bakken TPS. The Elm Coulee-Billings Nose Continuous Oil AU extends to the 5-ft isopach of the Middle Bakken to the south. The Central Basin Continuous Oil AU is delineated by the 450 mg HC/g TOC HI contour for the Upper Bakken that reflects oil maturity of this shale member. The Nesson-Little Knife Continuous Oil AU strictly follows the Nesson and Little Knife anticline structures. The Eastern Transitional Continuous Oil AU is defined by the 650 mg HC/g TOC HI contour to the west. Finally, the Northwest Transitional Continuous Oil AU is restricted by the 100-ohm resistivity line and mostly by the US-Canadian border [4].

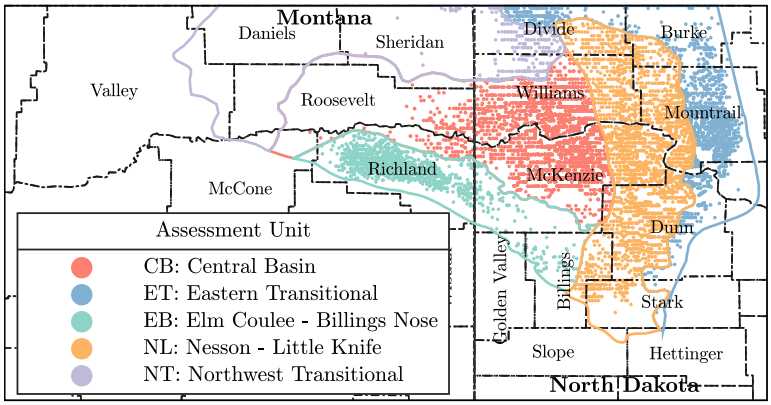

Figure 3. Map of the five assessment units (AU) for Bakken Total Petroleum System (TPS) in the Williston Basin introduced by USGS [4].

Preprints (www.preprints.org) | NOT PEER-REVIEWED | Posted: 25 December 2019 doi:10.20944/preprints201912.0334.v1

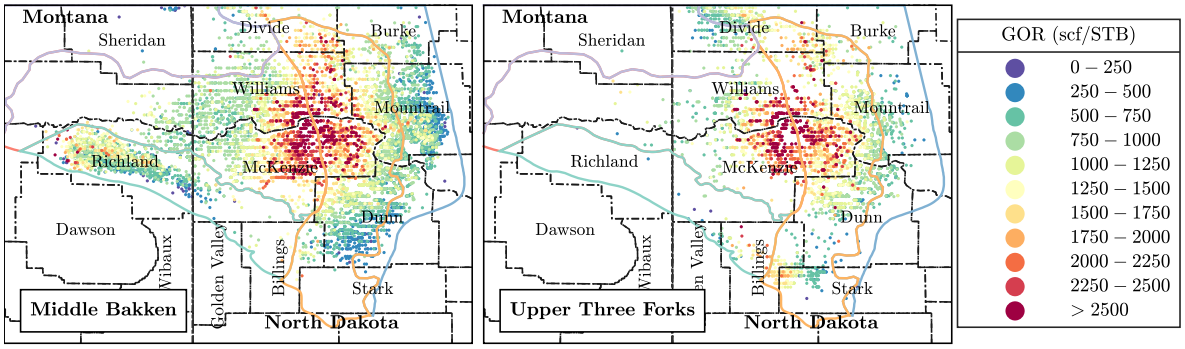

Figure 4. Maps of gas oil ratio (GOR) for all horizontal oil wells in the Middle Bakken and the Upper Three Forks . The red high GOR wells cluster in the central, most productive area in the Williston Basin.

About 75% of all active wells are located in the Nesson - Little Knife and the Central Basin, the two most productive AUs in the Bakken region. By mid-2019, the 14,888 Bakken wells were completed in two main reservoir layers: the Middle Bakken (9,894 wells) and the Upper Three Forks (4,994 wells). The maps of gas-oil ratio (GOR) and water cut (WC) in these two main layers are shown in Figure 4 and Figure 5. The high GOR wells are the red dots at the center, which is the most productive part of the Williston Basin. In the Bakken, operators are producing more oil than water in the Nesson anticline area, Parshall Field, and Elm Coulee Field. In the Three Forks formation water cut values are higher than those in the Bakken formation.

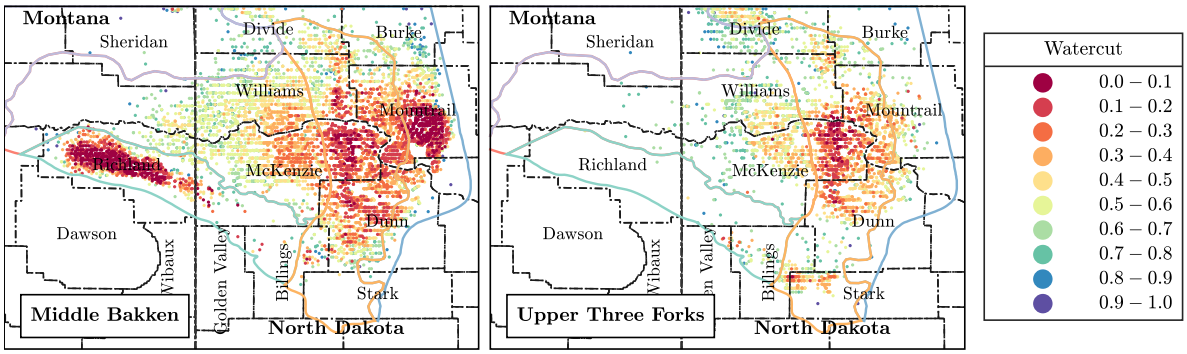

Figure 5. Map of water cut for all horizontal oil wells in the Middle Bakken and Upper Three Forks. The water cut values may also reflect maturity of the Lower Bakken and Upper Bakken shale layers in the Bakken petroleum system.

The GOR and WC contours may reflect maturity levels of the Bakken shale members and their productivity. The higher the GOR value, the more gas is dissolved in oil, giving more solution gas/compaction drive energy that increases oil recovery [27]. On the other hand, water cut is the ratio between water and total liquid production rates. WC is proportional to water saturation in the reservoir. A mature shale formation tends to have a low water cut and high GOR. The center of the basin seems to be the most productive region with a perfect combination of high GOR and low water cut. This particular area has the highest well density (the number of wells per square mile) that shows just how aggressive oil production strategy is in this most prolific part of the Bakken shale [33].

Preprints (www.preprints.org) | NOT PEER-REVIEWED | Posted: 25 December 2019 doi:10.20944/preprints201912.0334.v1

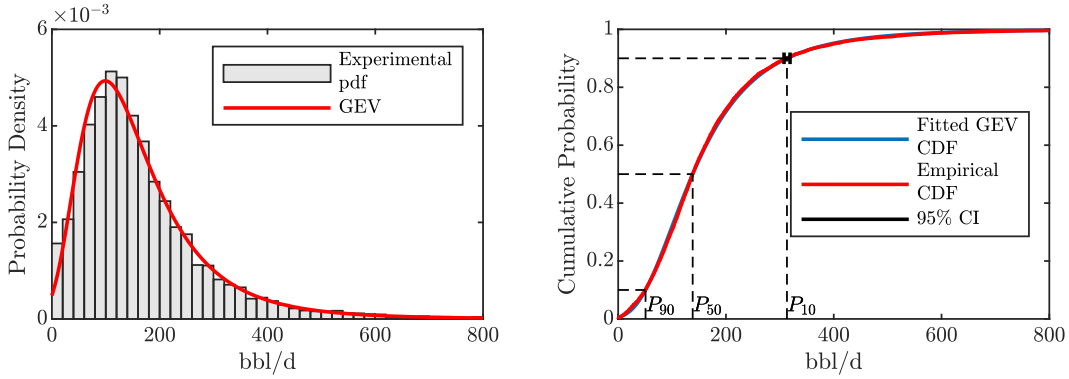

Figure 6. (Left) The probability density function (PDF) and **(Right)** the cumulative distribution function (CDF) of oil rate for the Bakken wells after 12 months on production [33,34]. The field data were fit with the generalized extreme value (GEV) distribution function that matches perfectly the experimental probability distributions. The P_{50} well is the expected value of the distribution, the P_{10} well is exceeded by only 10% of wells, and the P_{90} well is exceeded by 90% of wells.

A quick scoping analysis shows the distribution of oil rates from all Bakken wells after – in this example – one year on production, see Figure 6. This distribution is positively skewed, meaning that the majority of Bakken wells have low oil rates and the best wells with the significantly higher oil rates in the long tail are rare. The Generalized Extreme Value (GEV) distribution is most suitable to model the empirical oil rate distribution in the Bakken and other shales [33–35].

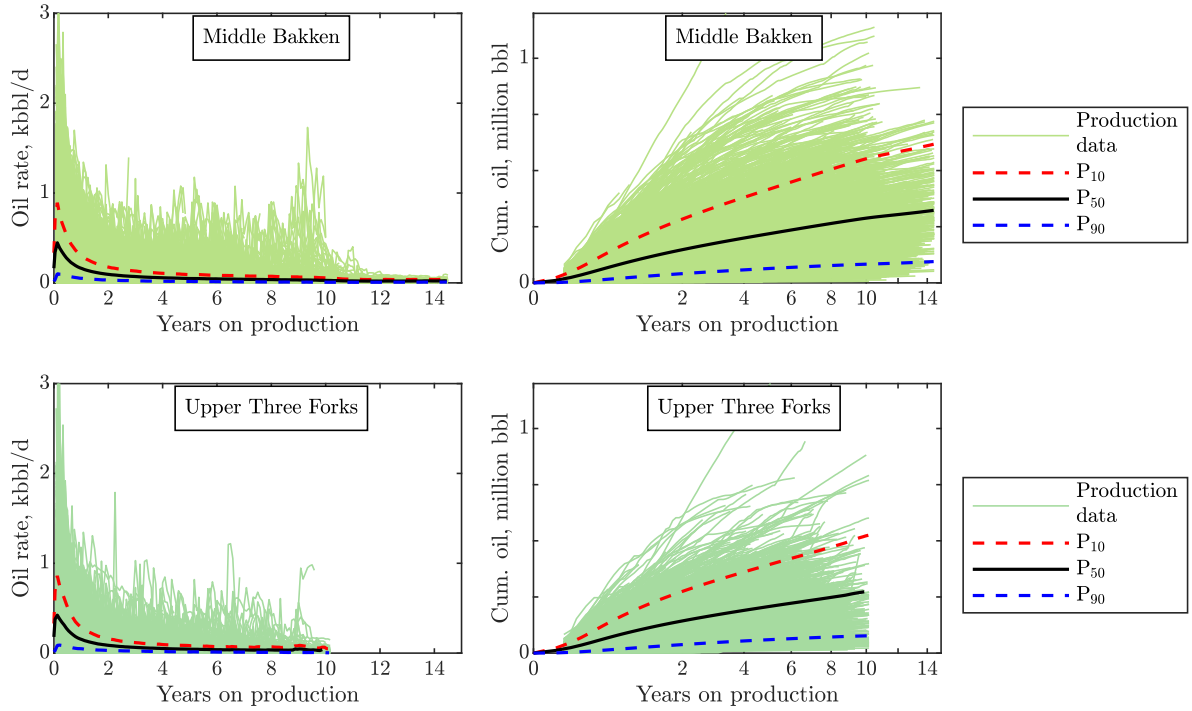

Figure 7. Daily oil rates and cumulative oil for the 14,888 horizontal oil wells in the Middle Bakken (9,894) and the Upper Three Forks (4,994). The P_{10}, P_{50}, and P_{90} wells are defined as 10%, 50%, and 90% of the cumulative distribution function (CDF) curves described in Figure 6.

Using the GEV statistics of well populations, we calculate the high (P_{10}), mean (P_{50}), and low (P_{90}), oil rate values from the cumulative distribution function (CDF). The P_{50} well is the expected value of the distribution; the P_{10} well is exceeded by only 10% of wells; and the P_{90} well is exceeded by 90% of wells. Figure 7 shows the daily oil rates and cumulative oil production for all existing horizontal wells in the Middle Bakken and the Upper Three Forks. Notice that the Three Forks wells

Preprints (www.preprints.org) | NOT PEER-REVIEWED | Posted: 25 December 2019 doi:10.20944/preprints201912.0334.v1

have fewer years on production because they were drilled after the year 2010. The P_{10}, P_{50}, and P_{90} wells were calculated with the method discussed elsewhere [33,34] and in the caption of Figure 6. The expected (P_{50}) maximum oil rate and cumulative oil are about 500 bbl/d and 200,000 bbl of oil for both Bakken and Three Forks. In addition, many production jumps are observed. Each jump is a sudden discontinuity of oil rate that is sometimes larger than the initial oil rate in the same well, and an abrupt brake in cumulative production curve. These discontinuities may be caused by refracturing of old wells [36–40] or by changes of downhole well flowing pressure [41–44].

3. Materials and Methods

3.1. Physical scaling

The physical scaling approach extended in this paper was first derived in the paper SPE-187226 [27], and used to predict oil production from thousands of horizontal wells in the Eagle Ford shale play. In several other papers, notably in [15,22,25,26,34,45], we have reviewed the vast literature on this subject and, to avoid repetition, we omit it here. The scaling solution given in SPE-187226 is based on an assumption that oil is produced from a hydrofractured shale well under a natural depletion mechanism (section 3.1.1). If a well intervention, most notably refracturing of old wells, occurs, this well's production cannot be scaled to a single master curve. Therefore, we implement superposition in time to address the erratic production records caused by well refracturing (section 3.1.2), or putting a well on artificial lift, or changing downhole flowing pressure, or a combination of two or more of these factors.

3.1.1. Physical scaling of natural depletion (SPE-187226)

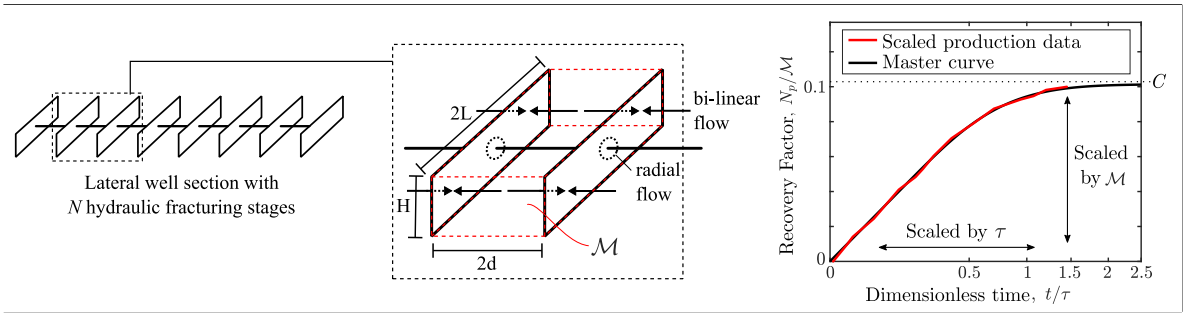

Figure 8. (Left) Illustration of bi-linear flow towards hydraulic fractures of a shale well. Reproduced from [27]. **(Right)** Illustration of the (almost) universal scaling curve method. The black line is the master curve that is the solution of the pressure diffusivity equation in hydrofractured well geometry. This master curve scales initially as the square root of time that later slows down due to exponentially declining rate of production. The constant C governs the vertical stretching of the master curve and can be calculated as $C = c_{ti}/S_{oi}(P_i - P_f)$. The cumulative mass produced by individual wells is then adjusted to match the master curve by a stretching/shrinking factor of $\mathcal{M}$ along the y-axis and τ along the x-axis. Reproduced from [28]

Figure 8 (left) illustrates the simple conceptual model used to derive our scaling method. The fracture height, H, is assumed to be the formation thickness; $2L$ is the tip-to-tip hydrofracture length; the one-sided area of hydrofracture, $A_f = 2L \times H$; and $2d$ is the distance between two consecutive hydraulic fractures (or stages). $\mathcal{M}$ is the mass of initial oil in place inside of the stimulated reservoir volume (SRV). In this model, radial flow into the wellbore is neglected, because the hydrofracture permeability is much higher than that of the rock matrix. As a result, we can assume bi-linear flow

Preprints (www.preprints.org) | NOT PEER-REVIEWED | Posted: 25 December 2019 doi:10.20944/preprints201912.0334.v1

towards hydraulic fracture planes and write a one-dimensional nonlinear pressure diffusion equation inside SRV. The oil production rate

$$q = -2\frac{kA_f}{\mu}\left(\frac{\partial p}{\partial x}\right)_{x=-d} \tag{1}$$

is obtained from the solution of the nonlinear – in general – oil pressure diffusion equation

$$\frac{\partial p}{\partial t} = \alpha(p)\frac{\partial^2 p}{\partial x^2} \tag{2}$$

with

$$\begin{aligned} \alpha(p) &= \frac{k}{\phi c_t \mu_o}\frac{\rho_o}{\rho_{\text{fluid}}} \\ c_t &= S_{oi}c_o + S_{wc}c_w + c_\phi \\ \rho_{\text{fluid}} &= \phi(S_o\rho_o + S_w\rho_w + S_g\rho_g), \quad \frac{\text{kg}}{\text{m}^3 \text{ bulk}} \end{aligned} \tag{3}$$

Here α is the pressure diffusivity coefficient that depends on the reservoir fluid pressure; ρ_{fluid} is the bulk density or reservoir fluid that may contain free gas in the near-hydrofracture regions; and c_t is the total system compressibility near bubble point pressure. For the derivation details, please see [27]

The initial and boundary conditions for this problem are

$$\begin{aligned} p(x, t=0) &= p_i, \text{ Initial pressure is uniform} \\ p(x \pm 1, t > 0) &= p_f, \text{ Hydrofracture pressure is constant} \\ &\text{during production} \end{aligned} \tag{4}$$

Briefly, with several assumptions that reflect the simplified physics of oil flowing mostly above the bubble point, the initial and boundary value problem (IBVP) (Equation (2) - Equation (4)) was solved analytically [27], and the following nonlinear least square optimization problem was obtained

$$\min_{\mathcal{M}>0,\tau>0} \mathcal{F}(\mathcal{M}, \tau, \dots) = \sum_{i=1}^{t_{\max}} \left[(\rho_{o,\text{ST}} + R_s\rho_{g,\text{ST}}q_{o,\text{ST}}(t_i))\Delta t_i - \frac{c_t(N\mathcal{M})}{S_{oi}}(p_i - p_f)\left(1 - \frac{8}{\pi^2}\sum_{n=0}^{\infty}\frac{1}{(2n+1)^2}\,\mathrm{e}^{(-(2n+1)^2\pi^2 t_i/(4\tau))}\right)\right]^2 \tag{5}$$

This problem has two unknowns,

$$\mathcal{M} = \rho_{oi}V = \rho_{oi}A_f(2d)\phi S_{oi} \tag{6}$$

and

$$\tau = \frac{d^2}{\alpha_i}, \text{ where } \alpha_i = \frac{k}{\phi c_t \mu_{oi}}\frac{\rho_{oi}}{\rho_{\text{fluid},i}} \tag{7}$$

where $\mathcal{M}$ is the initial mass of oil in place inside the stimulated reservoir volume between two consecutive hydraulic fractures; and τ is the characteristic time of pressure interference, or the square of interfracture half-distance, d, divided by the hydraulic diffusivity, α_i, at initial state of the reservoir. The parameter τ is the characteristic time needed for the depletion of oil pressure to diffuse to the midplane between two consecutive hydrofractures.

The complex non-linear optimization problem in Equation (5) is difficult to solve. Thus, a simpler but identical "physical scaling curve method" was introduced and illustrated in Figure 8 (right). This method consists of two steps. First, a master curve is constructed using Equation (8) with dimensionless

Preprints (www.preprints.org) | NOT PEER-REVIEWED | Posted: 25 December 2019 doi:10.20944/preprints201912.0334.v1

time, $\tilde{t} = \frac{t}{\tau}$, as the x-axis and dimensionless recovery factor, RF, as the y-axis. Second, *for each well*, its recorded cumulative produced mass is matched to the master curve by scaling the x-axis with τ and y-axis with $\mathcal{M}$.

$$\mathrm{RF}(\tilde{t}) = C\left(1 - \frac{8}{\pi^2}\sum_{n=0}^{\infty}\frac{1}{(2n+1)^2}\,\mathrm{e}^{(-(2n+1)^2\pi^2\tilde{t}/4)}\right) \tag{8}$$

with

$$C = \frac{c_t}{S_{oi}}(p_i - p_f) \tag{9}$$

being the ultimate oil recovery.

By performing this curve matching, the linearized oil pressure diffusion equation can be solved painlessly well-by-well, with the set of fit parameters, $\{\tau, \mathcal{M}\}$, providing key insights into the physics of production of the mostly saturated shale oil from thousands of wells. Finally, each EUR is calculated as the maximum recovery factor value from the master curve, $\mathrm{RF}(\tilde{t}_{\max})$, multiplied by the mass of oil in place, $\mathcal{M}$.

$$\mathrm{EUR} = \mathrm{RF}(\tilde{t}_{\max})\mathcal{M} = C\mathcal{M} \tag{10}$$

3.1.2. Physical scaling of well refracturing

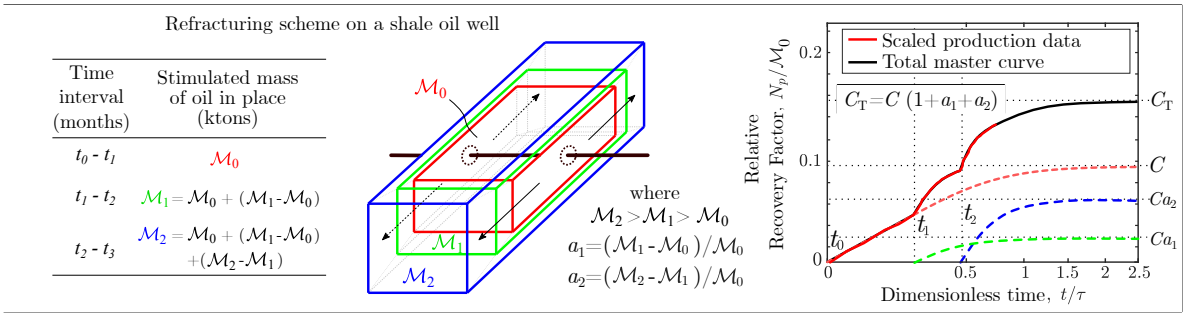

Figure 9. (**Left**) The refracturing process is illustrated as an increase of the stimulated reservoir volume (SRV) from $\mathcal{M}_0$ to $\mathcal{M}_1$ at time t_1; and from $\mathcal{M}_1$ to $\mathcal{M}_2$ at time t_2. (**Right**) A modification of the physical scaling curve coupled with superposition solves well refracturing problem. If primary production before refracturing has the recovery constant C (cf. Figure 8), then each refracturing event at t_j will start an imaginary well with the recovery constants $C \times a_j$. Here a_j scales the effectiveness of each fracturing job relative to the initial mass in place ($a_j = (\mathcal{M}_j - \mathcal{M}_{j-1})/\mathcal{M}_0$). Finally, the total master curve is scaled as $C_T = C(1 + a_1 + ... + a_n)$ to match the discontinuous historical production.

In many cases, the first hydraulic fracturing job is unsuccessful and results in a poor quality well that is a candidate for refracturing at a later time. Refracturing contributes to sudden jumps in production rate. The refracturing process is illustrated as an increase of the SRV in Figure 9 (left). As before, $\mathcal{M}$ is the initial mass of oil in place in the SRV. Before refracturing, the SRV box contains $\mathcal{M}_0$ ktons of oil in place. At time t_1, the first refracturing job is completed, and the mass in place jumps to $\mathcal{M}_1$. At t_2, the second refracturing job is performed, and an even bigger $\mathcal{M}_2$ is accessed. The refracturing process increases the mass $\mathcal{M}$ used to rescale cumulative oil production. By superposition theorem, this oil production is a summation of the production before refracturing that accessed the original mass in place, $\mathcal{M}_0$, and secondary production from imaginary wells at times t_j, $j = 1, 2, \ldots,$ that access the incremental masses in place, $(\mathcal{M}_j - \mathcal{M}_{j-1})$.

Preprints (www.preprints.org) | NOT PEER-REVIEWED | Posted: 25 December 2019 doi:10.20944/preprints201912.0334.v1

$$\min_{\mathcal{M}>0,\tau>0,a_j\geq 0} \mathcal{F}(\mathcal{M},\tau,a_j,\dots) = \sum_{i=1}^{t_{\max}} \left[\left(\rho_{o,\mathrm{ST}} + R_s\rho_{g,\mathrm{ST}}q_{o,\mathrm{ST}}(t_i)\right)\Delta t_i - \right.$$
$$\left. \sum_{j=0}^{n_{\mathrm{jump}}} \left(a_j \mathbb{H}_j \frac{c_t(N\mathcal{M}_0)}{S_{oi}}(p_i - p_f)\left(1 - \frac{8}{\pi^2}\sum_{n=0}^{\infty}\frac{1}{(2n+1)^2}\mathrm{e}^{\left(-(2n+1)^2\pi^2|t_i-t_j|/(4\tau)\right)}\right)\right)\right]^2 \tag{11}$$

The production jumps from refracturing cannot be scaled with the standard master curve shown in Figure 8. Thus, we combine the physical scaling solution with superposition and obtain Equation (11) that remedies this difficulty. If primary production before refracturing has the recovery constant C in Equation (12), then each refracturing event j at time t_j activates an imaginary well with the recovery constant $C \times a_j$. Here a_j's are the new fitting parameters that scale effectiveness of each refracturing job relative to the initial mass in place, Equation (13). $\mathbb{H}_j$ is the Heaviside step function that handles time delays in the consecutive refracturing jobs.

$$C = \frac{c_t}{S_{oi}}(p_i - p_f) \tag{12}$$

$$a_j = \frac{\mathcal{M}_j - \mathcal{M}_{j-1}}{\mathcal{M}_0} \tag{13}$$

$$\mathbb{H}_j = \begin{cases} 0, & t_i - t_j < 0, \\ 1, & t_i - t_j \geq 0, \end{cases} \tag{14}$$

The total master curve RF_T is the summation of all individual master curves, RF_j, see Equation (15) and Equation (16). An example of matching the scaled discontinuous historical production is shown in Figure 9 (right).

$$\mathrm{RF}_T(\tilde{t}) = \sum_{j=0}^{n_{\mathrm{jump}}} \mathrm{RF}_j(\tilde{t}) \tag{15}$$

$$\mathrm{RF}_j(\tilde{t}) = a_j\mathbb{H}_j C\left(1 - \frac{8}{\pi^2}\sum_{n=0}^{\infty}\frac{1}{(2n+1)^2}\mathrm{e}^{\left(-(2n+1)^2\pi^2\tilde{t}/4\right)}\right), \text{ where } \tilde{t} = \frac{|t_i - t_j|}{\tau} \tag{16}$$

Finally, one calculate EUR by multiplying the maximum total recovery factor from the modified master curve, $\mathrm{RF}_T(\tilde{t}_{\max})$, with the initial mass of oil in place before fracturing, $\mathcal{M}_0$, Equation (17).

$$\mathrm{EUR}_T = \mathrm{RF}_T(\tilde{t}_{\max})\mathcal{M}_0 = C\left(1 + \sum_{j=1}^{n_{\mathrm{jump}}} a_j\right)\mathcal{M}_0 \tag{17}$$

3.2. Data collection and scaling procedure

We have mined public well records for the Bakken shale from the DrillingInfo (now Enverus) database, the Montana Department of Natural Resources and Conservation - Board of Oil and Gas Conservation website, and the North Dakota Department of Mineral Resources - Oil and Gas Division website with a premium subscription. In DrillingInfo, we have selected only 14,888 horizontal oil wells that were completed after Jan 1, 2000, in the Middle Bakken and Three Forks formations. The raw production data from DrillingInfo were imported into an integrated MATLAB® software package we designed to perform data cleanup, consolidation, and unit conversions. The clean production data for each well consist of a vector of elapsed time on production (consecutive months with nonzero oil volume records) and a vector of cumulative oil production in kilotons.

Preprints (www.preprints.org) | NOT PEER-REVIEWED | Posted: 25 December 2019 doi:10.20944/preprints201912.0334.v1

Our scaling procedure of obtaining EUR for each well is as follows:

1. Exclude all *newly completed wells* with less than 12 months of production).
2. For each remaining well, plot its cumulative production vs. square root of time on production. Classify these wells as:
   (a) *Non-interfering wells*, if the plot shows a straight line (with, e.g., $R^2 \geq 0.9$).
   (b) *Interfering wells*, if the plot shows a deviation from a straight line (with, e.g., $R^2 < 0.9$)
   (c) *Refrac wells*, if production jumps are detected.
3. For each non-interfering well, scale its cumulative production by $\mathcal{K}\sqrt{t_{\max}}$, on the $y-$axis and the elapsed time on production by $t_{\max}$ on the $x-$axis to match the line $f(\tilde{t}) = \sqrt{\tilde{t}}$. To predict EUR, assume – somewhat optimistically – that deviation from the line starts at $\tau = 2 \times t_{\max}$. Thus, the corresponding $\mathcal{M}$ can be calculated as $\mathcal{M} = (\mathcal{K}\sqrt{t_{\max}})/\mathrm{RF}(\frac{1}{2})$, where $\mathrm{RF}(\frac{1}{2})$ is calculated from Equation (8). Finally, EUR is calculated from Equation (10).
4. For each interfering well, scale its cumulative production records to the master curve in Equation (8) using two scaling parameters, τ and $\mathcal{M}$. The corresponding EURs are calculated from Equation (10).
5. For each refrac well, scale its cumulative production records to the master curve in Equation (15), and obtain optimum values of the scaling parameters τ, $\mathcal{M}_0$, and a_j, $j = 1, 2, \ldots$. The corresponding EURs are calculated from Equation (17).
6. For each newly completed well, calculate its EUR using expected values of τ and $\mathcal{M}$ from comparable interfering wells that were completed between 2017 and 2018. Use Equation (10).

Notice that the EURs calculated from Equation (10) and Equation (17) are in mass units. We use oil density to convert these EURs into thousands or millions of barrels (kbbl or Mbbl).

4. Results and Discussion

4.1. Physical scaling matches

We have scaled oil production from all 14,888 horizontal oil wells in the Bakken following procedure detailed in section 3.2. The reservoir properties used in scaling oil production are listed in Table A1. The key scaling results are shown in Figure 10 – Figure 12.

At the time of this analysis, 4,845 Bakken wells, 3,349 in the Middle Bakken and 1,496 in the Upper Three Forks, were classified as *non-interfering wells*, because their cumulative production was still growing linearly versus the square root of time. Notice that the x-axis in Figure 10 is scaled with the maximum time on production, $t_{\max}$ instead of τ and the y-axis is scaled with $\mathcal{K}\sqrt{t_{\max}}$ to match the $f(\tilde{t}) = \sqrt{\tilde{t}}$ master curve that intersects point (1,1). In the Middle Bakken, the expected values of $t_{\max}$ and $\mathcal{K}\sqrt{t_{\max}}$ are 75 months and 30 ktons, while in Three Forks these values are 65 months and 27 ktons. For the non-interfering wells, we assume arbitrarily that they start to decline exponentially (go under the square-root of time linear trend) at $\tau = 2 \times t_{\max}$.

The *interfering wells* exhibit clear pressure-interference between consecutive hydrofractures. For each well k, this interference already occurred at the elapsed time on production $t = \tau_k$ and, at the time of this analysis, each oil production rate was declining exponentially. For these wells, the recovery factors start bending down at the dimensionless time equal $0.5 < 0.64$ in [25] because oil is less compressible than gas. The interfering wells scale with the master curve in Figure 8. Of the 6,401 interfering wells in the Bakken, 4,245 were in the Middle Bakken and 2,156 in the Upper Three Forks (Figure 11). The expected values of τ and $\mathcal{M}$ were 100 months and 420 ktons for the Middle Bakken, and 90 months and 320 ktons for the Upper Three Forks.

Many wells in the Bakken (2,363) cannot be scaled to a non-interfering or interfering segment of the scaling curve. The poor matches are caused by multiple production jumps that may be due to refracturing of old wells [36–40]. We note that these jumps could also result from artificial lift and step decreases of downhole well pressure [41–44]. Each of these wells is scaled individually with a modification of the full physical scaling curve coupled with superposition, see Figure 9. Four

Preprints (www.preprints.org) | NOT PEER-REVIEWED | Posted: 25 December 2019 doi:10.20944/preprints201912.0334.v1

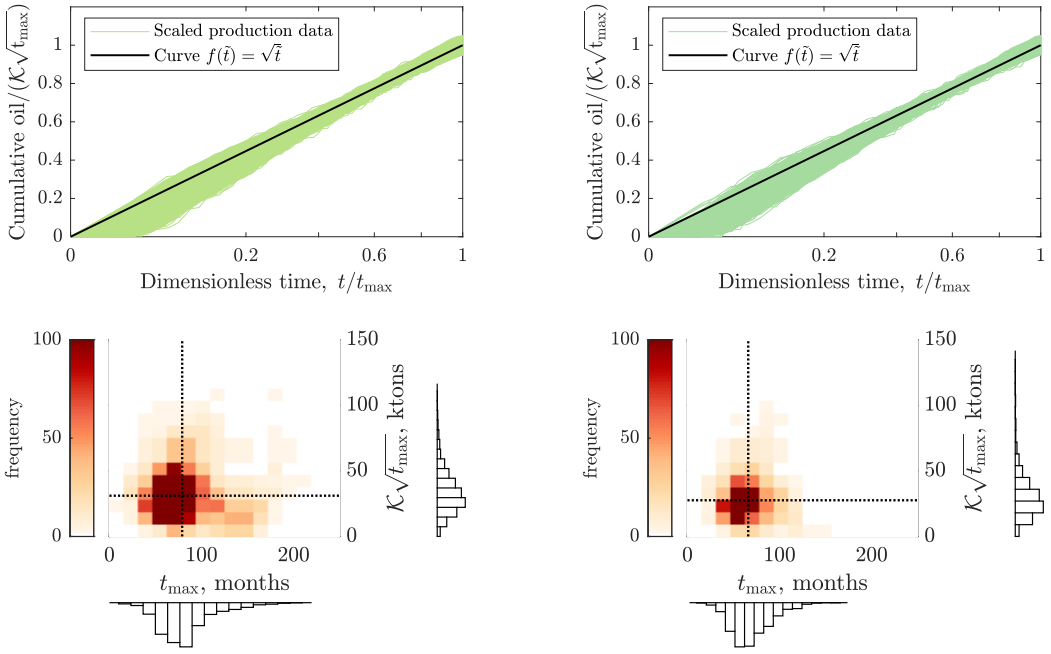

(a) Middle Bakken **(b)** Upper Three Forks

Figure 10. The physical scaling matches of 4,845 non-interfering wells: 3,349 in the Middle Bakken and 1,496 in the Three Forks with the corresponding $\mathcal{K}\sqrt{t_{\max}}$ and $t_{\max}$ distributions.

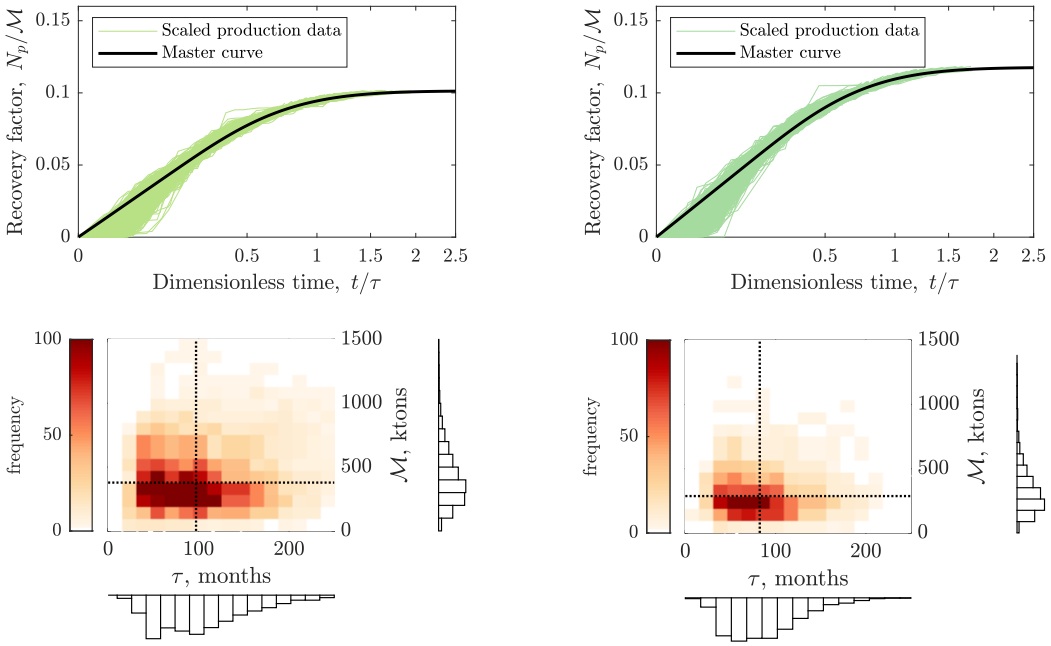

(a) Middle Bakken **(b)** Upper Three Forks

Figure 11. The physical scaling matches of 6,401 interfering wells: 4,245 in the Middle Bakken and 2,156 and the Three Forks with the corresponding $\mathcal{M}$ and τ distributions.

Preprints (www.preprints.org) | NOT PEER-REVIEWED | Posted: 25 December 2019 doi:10.20944/preprints201912.0334.v1

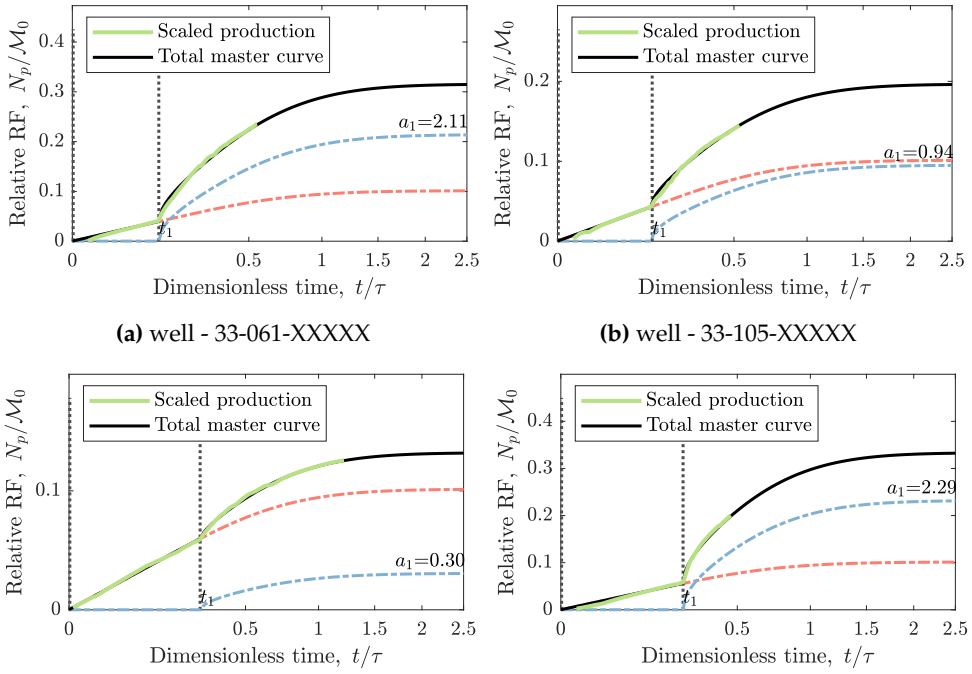

(a) well - 33-061-XXXXX **(b)** well - 33-105-XXXXX

(c) well - 25-083-XXXXX **(d)** well - 33-025-XXXXX

Figure 12. Example of physical scaling matches for refrac wells.

examples of "refrac wells" are shown in Figure 12. The two wells in the left panels are completed in the Middle Bakken formation, while the two wells on the right are completed in the Upper Three Forks formation. As we can see, the modified scaling curve matches the discontinuous production records. The magnitude of each a in Equation (13) may reflect effectiveness of a specific refracturing job. For all "refrac wells," the expected value of a is about 0.6, a little better than 50%.

The remaining 1,279 *newly completed wells* had less than 12 months on production at the time of this analysis. The oil production rates from these wells are usually unstable due to back flow of fracturing fluids, excessive choking and/or lack of takeaway capacity [25,26,46–50].

During the first three months on production in each well, the produced cumulative oil volume is commonly below the square-root-of-time line due to the unloading of SRV from fracturing fluids, whose flow blocks oil production, [25,26]. If a well does not have enough stable production history, its scaling will underestimate both τ and $\mathcal{M}$. Therefore, we have decided to use the average τ and $\mathcal{M}$ values from scaling the recently completed (in 2017–2018) interfering wells with $\tau = 45$ months and $\mathcal{M} = 495$ ktons for the Middle Bakken and 43 months and 390 ktons for the Upper Three Forks. Notice that the magnitude of τ is lower and that of $\mathcal{M}$ is higher for the new wells. These shifts are caused by the improvements of well completion technology, i.e., by bigger hydrofractures, fewer clusters per stage, more fracture stages, etc., over the last decade [51–57].

Table A2 details the interference times, τ, and the masses of oil in place, $\mathcal{M}$, for the four well classes: 1) interfering, 2) non-interfering, 3) refracs, and 4) newly completed wells in the Middle Bakken and Upper Three Forks. The surface location maps of these four well classes are shown in Figure 13 for both reservoirs. For the Middle Bakken, wells in the first three classes spread extensively from the center of the Williston Basin in North Dakota to the Elm Coulee Field in Montana, while in the Three Forks few wells were drilled in Montana. Interestingly, the newly completed wells are located mostly in the central part of the Williston Basin in North Dakota. There were some new wells completed in Montana; however, they became inactive within the first few months on production. In general, the magnitudes of τ and $\mathcal{M}$ in the Upper Three Forks are lower than those in the Middle Bakken, indicating that the Three Forks wells decline faster and have lower EURs than those in the Middle Bakken. The refrac wells have the highest values of $\mathcal{M}$, because of the incremental stimulated reservoir

Preprints (www.preprints.org) | NOT PEER-REVIEWED | Posted: 25 December 2019 doi:10.20944/preprints201912.0334.v1

volumes due to refracs. The non-interfering wells have slightly higher EURs than the interfering wells, because of the larger τ and $\mathcal{M}$ values. As mentioned before, the newly completed wells have shorter τs and larger $\mathcal{M}$s than all other well classes. Each of these wells starts from a very high initial production rate that declines very fast.

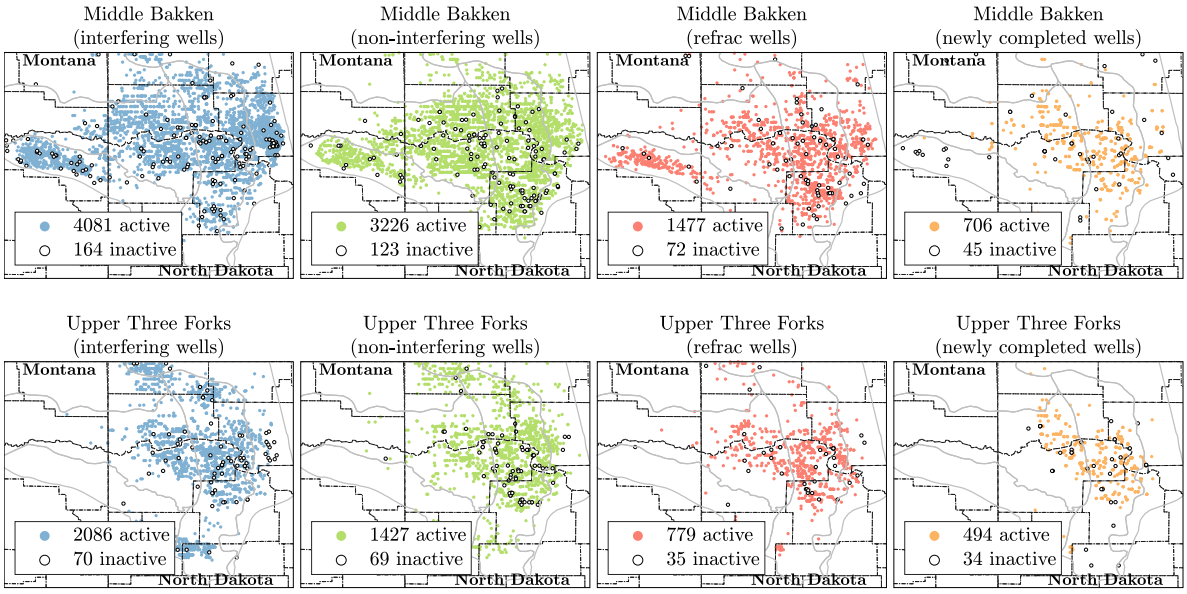

Figure 13. Different classes of the 14,888 horizontal wells in the Middle Bakken and Upper Three Forks. There are 6,401 interfering wells, 4,845 non-interfering wells, 2,363 "refrac" wells, and 1,279 new wells that have less than 12 months on production. The filled circles show the surface location of active wells in each class, while the empty circles denote inactive wells.

4.2. EUR predictions

To predict the fieldwide EUR, all individual scaling curves for the 14,888 existing wells in the Bakken are summed up vs calendar time (Figure 14). For each well class, we note the high fidelity of the physical scaling approach in retracing old production and – by implication – forecasting future production of the existing wells. From Figure 14 (left), we infer that the second production peak in the last three years is not only the contribution from the newly completed wells that are highly productive, but also from the old wells that have been refractured or pumped off recently. From Figure 14 (right), it follows that the expected estimated ultimate recovery from all 14,888 wells in the Bakken play is about 4.5 billion bbl of oil. The EURs for the interfering and non-interfering well classes are almost the same at about 1.5 billion bbl each, as the respective well numbers are close: 6,401 and 4,845. The refrac wells have a larger average EUR per well with total EUR of 1 billion bbl from only 2,363 wells. The recent 1,279 wells also have a higher EUR per well with the total EUR of 0.5 billion bbl. One can argue that success of the newly completed wells in yielding the highest EURs is not only due to the significant improvements in well completion techniques, but also to the favorable drilling location selections across the most prolific area in the Bakken, near the center of the Williston Basin (recall Figure 13).

In order to compare our results with EUR predictions from the US DOE Energy Information Administration [6], we have remapped each Bakken assessment unit onto counties and calculated the expected value of EUR for each county. The details are tabulated in Table A3. We predict the EUR from all 14,888 active horizontal oil wells in the Bakken to be 4.5 billion barrels of oil (~300 kbbl/well), with 3.1 billion barrels coming from 9,894 wells in the Middle Bakken (309 kbbl/well) and 1.4 billion barrels coming from 4,994 wells in the Upper Three Forks (278 kbbl/well). The results in Table A3 are also displayed as stacked bar graphs for the Middle Bakken and the Upper Three Forks (Figure 15). The stacked bars show the numbers of existing wells from the DrillingInfo dataset in 2019, and the *potential* wells from [6] in each Bakken TPS assessment unit mapped onto the corresponding counties in the

Preprints (www.preprints.org) | NOT PEER-REVIEWED | Posted: 25 December 2019 doi:10.20944/preprints201912.0334.v1

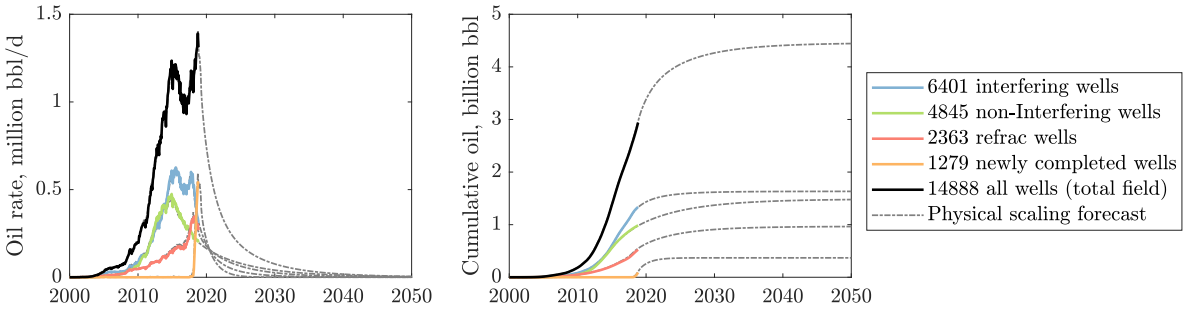

Figure 14. Historical production data and the physical scaling projection for all horizontal wells in the Middle Bakken and Upper Three Forks. To match the historical oil rate and cumulative oil in the Bakken formation, all individual scaling curves for the 14,888 wells are summed up vs calendar time.

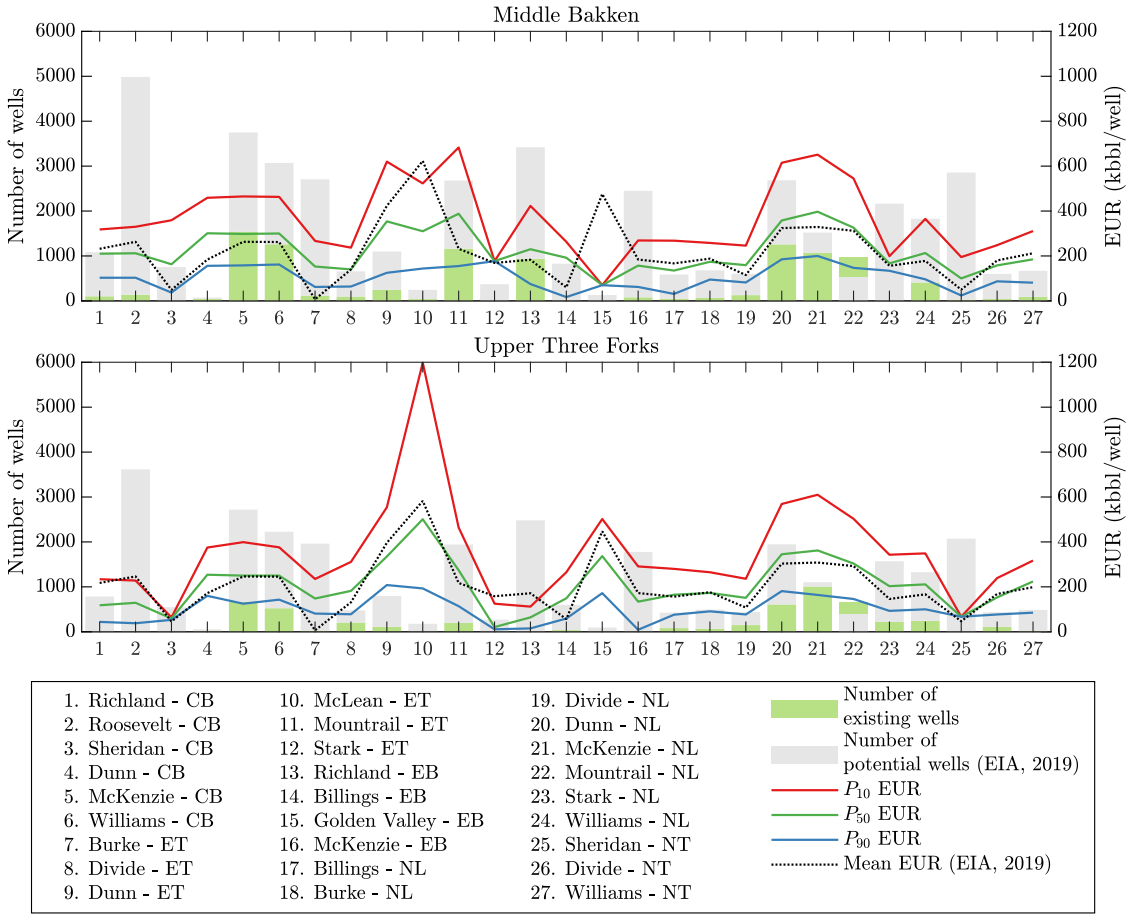

Figure 15. The stacked bars show the numbers of existing wells from the DrillingInfo dataset in 2019, and the *potential* wells from the EIA report [6] in each Bakken TPS assessment unit mapped onto the corresponding counties in the Middle Bakken and Upper Three Forks Formations. The lines show the corresponding EUR values from the physical scaling and the EIA statistical predictions. The P_{10}, P_{50}, and P_{90} wells were obtained by applying the generalized extreme value (GEV) distribution for each set of EURs from the scaling curve method in each sub-region. For the counties with a large number of existing wells, the P_{50} values, the EIA predictions are close enough to our scaling.

Preprints (www.preprints.org) | NOT PEER-REVIEWED | Posted: 25 December 2019 doi:10.20944/preprints201912.0334.v1

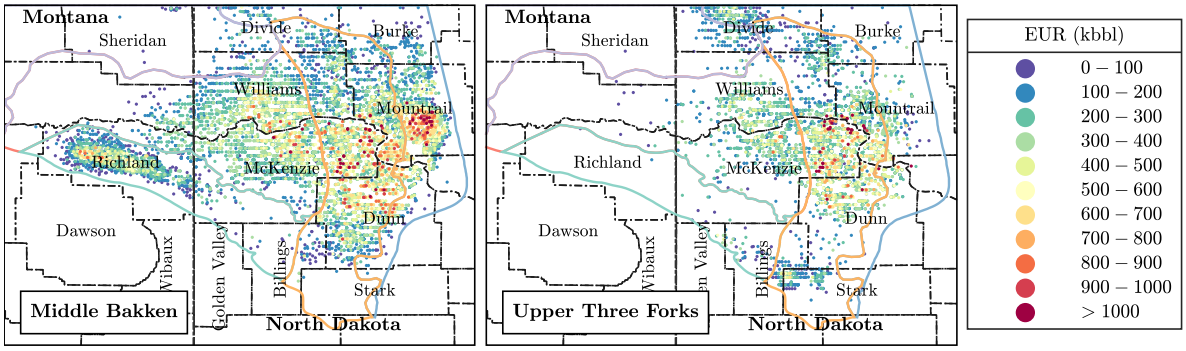

Figure 16. A map of EURs obtained from the universal scaling curve method for 14,888 horizontal wells in Bakken shale. Notice that this map resembles the water cut map, rather than the GOR map. This indicates that EUR is negatively correlated with water cut.

Middle Bakken and Upper Three Forks Formations. The lines show the corresponding EUR values from the physical scaling and the EIA statistical predictions. The P_{10}, P_{50}, and P_{90} wells were obtained by applying the generalized extreme value (GEV) distribution [33,34] for each set of EURs from the scaling curve method in each sub-region as demonstrated before in Figure 6. In most cases, where there are enough wells per sample, the expected P_{50} EURs from physical scaling agree with the EUR estimates by EIA. One can observe that most of the best regions with the high EUR values have been extensively drilled leaving no or few potential wells to infill. *Mountrail - NL* is an extreme example of over-drilling in the best region of the Bakken, where the number of existing wells exceeds the number of EIA potential wells by 40% (the green bar is taller than the gray bar). In another paper [33], we have calculated well density of all regions in the Bakken, revealing a surprising result that the core area of the Bakken will be fully drilled by 2021. In contrast, most of the 85,334 potential wells proposed by EIA will be located in the poorest regions of the Bakken. Figure 16 maps the EUR results from physical scaling approach for 14,888 horizontal oil wells in the Bakken. Notice that this map resembles more the water cut map (Figure 5), rather than the GOR map (Figure 4).

In Figure 17 (left), we show that EUR is negatively correlated with water cut (1 − oil cut). On the other hand, there is little correlation between EUR and lateral length, as depicted in Figure 17 (right). Doubling lateral length from 5,000 to 10,000 ft does not double average EUR that increases from 240 to just 310 kbbl. This finding may also suggest that better technology cannot increase EUR if a well is drilled in a low-productivity region of the Bakken.

Figure 18 shows the average values of pressure interference time, τ, lateral length, gas oil ratio, and water cut for each six-month time interval in calendar dates. The value of τ decreases significantly over time meaning that newer wells pressure-interfere and decline faster than the old ones. Equation (7) shows that τ is directly proportional to the square of half-distance, d, between two consecutive hydrofractures. This means that halving the interfracture distance decreases τ four-fold. Historically, the number of hydrofracture stages in the Bakken has increased over time from 8 stages in 2007 [54], to 18 stages in 2009 [55], 35 stages in 2016 [56], and to as many as 60 stages in 2019 [57]. The lateral length has also doubled from 5,000 ft in 2005 to 9500 ft in 2015.

In summary, the new completion techniques in the Bakken shale rely on more of bigger hydraulic fractures and on longer laterals [51–53]. These new completions have significant side-effects. Cumulative gas-oil-ratio has been increasing in both the Middle Bakken and Three Forks. The likely culprits are reservoir depressuring by hydrofractures that are too close and the increasingly aggressive artificial lift. Degassing the low permeability and porosity reservoirs in the Bakken spells trouble for future production, because solution- and free gas are the main driving mechanisms of primary depletion. Water cut has also increased with time revealing another negative side-effect of the recent Bakken field development. The increasing water cut might be caused by drilling new low productivity

Preprints (www.preprints.org) | NOT PEER-REVIEWED | Posted: 25 December 2019 doi:10.20944/preprints201912.0334.v1

wells in the immature regions of Bakken [29,30,58], and/or by the longer and taller hydraulic fractures that break into adjacent water-bearing formations, the Lodgepole and/or Lower Three Forks [59–61].

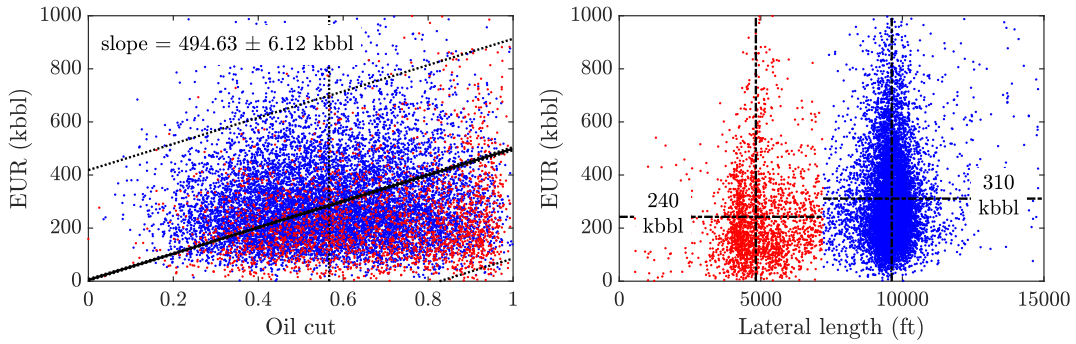

Figure 17. Scatter plot of EURs vs oil cut (left) and EUR vs lateral length (right) for all 14,888 horizontal oil wells in Bakken. In most cases, a lower oil cut (higher water cut), corresponds to a lower EUR. On the other hand, there is no direct correlation between EUR and lateral length. The group of short lateral wells, 5,000 feet long, has both high and low EUR values, while the group of the long lateral wells, 10,000 feet long, also has high and low EURs.

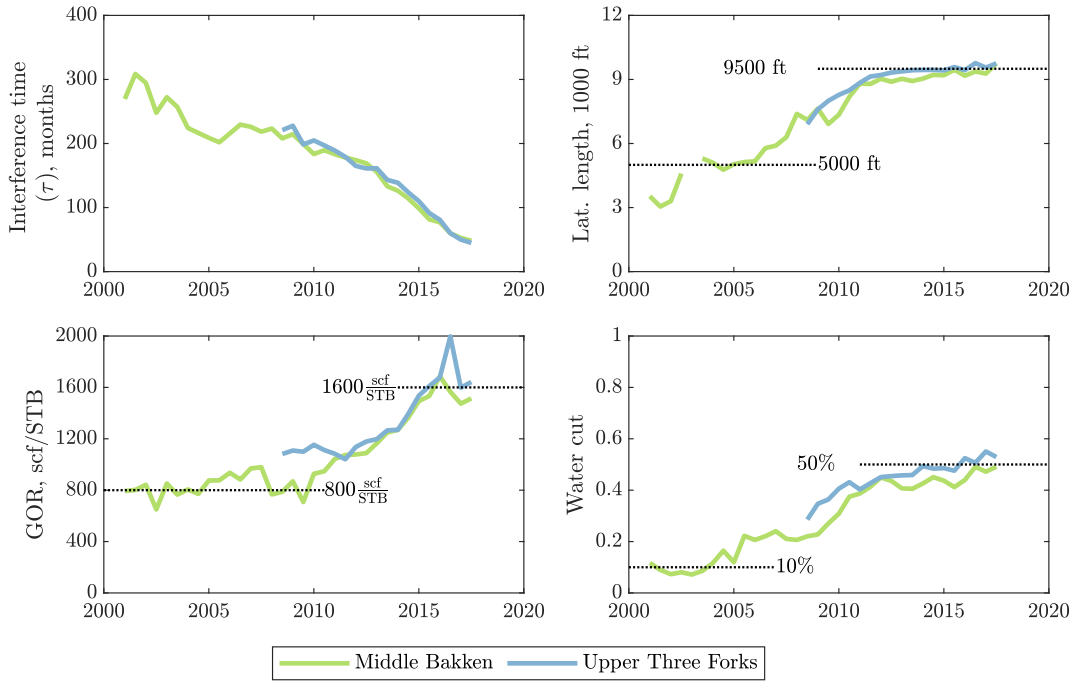

Figure 18. From left to right: **(1)** Average pressure interference time, τ in months vs calendar time for the Middle Bakken and Upper Three Forks. The τ values decrease with time, indicating perhaps advances in the completion technology that result in more fracture stages with bigger hydrofractures in each newer well. (**2**) Average lateral length vs calendar time shows that old wells have short laterals averaging 5,000 ft, while the recent wells are longer at about 10,000 ft. (**3**) Average gas-oil ratio (GOR) vs calendar time shows a positive trend for both Middle Bakken and Upper Three Forks. In the beginning, Three Forks produced slightly more gas. (**4**) Average water-cut vs calendar time also shows a positive trend for the Middle Bakken and Upper Three Forks. The Three Forks wells produce slightly more water than the Middle Bakken ones.

5. Conclusions

We have delivered a comprehensive physics-based scaling of all horizontal hydrofractured wells completed in the Middle Bakken and Upper Three Forks between Jan 1 2000, and May 1 2019. In particular:

- The current 14,888 active oil wells in the Bakken shale will ultimately produce 4.5 billion barrels of oil (0.3 Mbbl/well), with 3.1 billion barrels from 9,894 wells in the Middle Bakken and 1.4 billion barrels from 4,994 wells in the Upper Three Forks.
- By March 2020, total oil production rate from these 14,888 wells will decline to one-half of the production peak in late 2018.
- In general, wells completed in the Middle Bakken layer produce more oil than those in the Upper Three Forks layer due to: 1) lower water saturation and water cut, 2) slower decline rate (longer pressure interference times, τ), and 3) higher initial oil in place (larger $\mathcal{M}$).
- Newly completed wells start from very high initial oil rates but in general decline faster than the pre-2010 wells. Still, we predict higher EURs for the newly completed wells.
- The more productive newer wells result from recent advancements in completion technology: longer laterals, larger hydrofractures, bigger stimulated reservoir volumes, and more fracture stages.
- Operators have also learned to drill new wells only in the most prolific area of the Bakken region at the center of the Williston Basin.
- With time, negative trends in oil production have amplified in the Bakken. We observe higher GOR values (reservoir degassing); higher water cuts (contacting water-bearing formations and drilling in regions with lower oil saturations); faster decline rates; and excessive well density, especially in the most prolific areas.
- After all most productive areas in the Bakken are extensively drilled, the poor immature areas with high water production will be the only targets left for infill drilling. In this case, technology will not enhance much performance of the future wells.
- We encourage practitioners to adopt our fast and accurate method of predicting oil production in shales that is a viable alternative to the hyperbolic DCA which yields an 'illusory picture' of shale oil resources.

Elsewhere [33], we outline a hybrid method that combines the precise GEV statistics of horizontal oil wells in the Bakken with the physics-based scaling method developed in this paper and combined with late-time inflow [45]. This hybrid approach follows from our comprehensive evaluation of the Barnett play futures [34].

Acknowledgement

The authors thank the Ali I. Al-Naimi Petroleum Engineering Research Center (ANPERC) at KAUST for funding this project.

References

1. Medeiros, F.; Ozkan, E.; Kazemi, H. Productivity and Drainage Area of Fractured Horizontal Wells in Tight Gas Reservoirs. Rocky Mountain Oil & Gas Technology Symposium. Society of Petroleum Engineers, 2007. doi:10.2118/108110-ms.
2. Ikonnikova, S.; Browning, J.; Horvath, S.C.; Tinker, S. Well Recovery, Drainage Area, and Future Drill-Well Inventory: Empirical Study of the Barnett Shale Gas Play. *SPE Reservoir Evaluation & Engineering* **2014**, *17*, 484–496. doi:10.2118/171552-pa.
3. Arps, J. Analysis of Decline Curves. *Transactions of the AIME* **1945**, *160*, 228–247. doi:10.2118/945228-g.
4. Gaswirth, S.B.; Marra, K.R.; Cook, T.A.; Charpentier, R.R.; Gautier, D.L.; Higley, D.K.; Klett, T.R.; Lewan, M.D.; Lillis, P.G.; Schenk, C.J. Assessment of undiscovered oil resources in the bakken and three forks

formations, Williston Basin Province, Montana, North Dakota, and South Dakota, 2013. *US Geological Survey Fact Sheet* **2013**, *3013*.

5. Cook, T.A. Procedure for Calculating Estimated Ultimate Recoveries of Bakken and Three Forks Formations Horizontal Wells in the Williston Basin. Open-File Report 2013–1109, USGS, 2013.
6. EIA. Assumptions to the Annual Energy Outlook 2019: Oil and Gas Supply Module. *US Energy Information Administration: Annual Energy Outlook* **2019**, p. 7.
7. Kanfar, M.; Wattenbarger, R. Comparison of Empirical Decline Curve Methods for Shale Wells. SPE Canadian Unconventional Resources Conference. Society of Petroleum Engineers, 2012. doi:10.2118/162648-ms.
8. Tan, L.; Zuo, L.; Wang, B. Methods of Decline Curve Analysis for Shale Gas Reservoirs. *Energies* **2018**, *11*, 552. doi:10.3390/en11030552.
9. Olson, B.; Elliott, R.; Mathhews, C.M. Fracking's Secret Problem–Oil Wells Aren't Producing as Much as Forecast. *The Wall Street Journal* **January 2, 2019**.
10. Lapierre, S. On the Nature and Character of the Widespread Oil Production Shortfalls Reported by the Wall Street Journal. *Linkedin Pulse* **September 11, 2019**.
11. Ilk, D.; Rushing, J.A.; Perego, A.D.; Blasingame, T.A. Exponential vs. Hyperbolic Decline in Tight Gas Sands: Understanding the Origin and Implications for Reserve Estimates Using Arps& Decline Curves. SPE Annual Technical Conference and Exhibition. Society of Petroleum Engineers, 2008. doi:10.2118/116731-ms.
12. Valko, P.P. Assigning value to stimulation in the Barnett Shale: a simultaneous analysis of 7000 plus production hystories and well completion records. SPE Hydraulic Fracturing Technology Conference. Society of Petroleum Engineers, 2009. doi:10.2118/119369-ms.
13. Valko, P.P.; Lee, W.J. A Better Way To Forecast Production From Unconventional Gas Wells. SPE Annual Technical Conference and Exhibition. Society of Petroleum Engineers, 2010. doi:10.2118/134231-ms.
14. Duong, A.N. Rate-Decline Analysis for Fracture-Dominated Shale Reservoirs. *SPE Reservoir Evaluation & Engineering* **2011**, *14*, 377–387. doi:10.2118/137748-pa.
15. Clark, A.J.; Lake, L.W.; Patzek, T.W. Production Forecasting with Logistic Growth Models. SPE Annual Technical Conference and Exhibition. Society of Petroleum Engineers, 2011. doi:10.2118/144790-ms.
16. Gong, X.; Gonzalez, R.; McVay, D.A.; Hart, J.D. Bayesian Probabilistic Decline-Curve Analysis Reliably Quantifies Uncertainty in Shale-Well-Production Forecasts. *SPE Journal* **2014**, *19*, 1047–1057. doi:10.2118/147588-pa.
17. Paryani, M.; Awoleke, O.O.; Ahmadi, M.; Hanks, C.; Barry, R. Approximate Bayesian Computation for Probabilistic Decline-Curve Analysis in Unconventional Reservoirs. *SPE Reservoir Evaluation & Engineering* **2017**, *20*, 478–485. doi:10.2118/183650-pa.
18. Zhang, H.; Rietz, D.; Cagle, A.; Cocco, M.; Lee, J. Extended exponential decline curve analysis. *Journal of Natural Gas Science and Engineering* **2016**, *36*, 402–413. doi:10.1016/j.jngse.2016.10.010.
19. Yu, S. A Comprehensive Study of b-Values for Proven Reserve Estimation Using Hyperbolic Decline for Vertical Commingled Gas Producers in Deep Basin Area of WCSB. SPE/CSUR Unconventional Resources Conference. Society of Petroleum Engineers, 2015. doi:10.2118/175889-ms.
20. Stumpf, T.N.; Ayala, L.F. Rigorous and Explicit Determination of Reserves and Hyperbolic Exponents in Gas-Well Decline Analysis. *SPE Journal* **2016**, *21*, 1843–1857. doi:10.2118/180909-pa.
21. Sharma, P.; Salman, M.; Reza, Z.; Kabir, C. Probing the roots of Arps hyperbolic relation and assessing variable-drive mechanisms for improved DCA. *Journal of Petroleum Science and Engineering* **2019**, *182*, 106288. doi:10.1016/j.petrol.2019.106288.
22. Ogunyomi, B.A.; Patzek, T.W.; Lake, L.W.; Kabir, C.S. History Matching and Rate Forecasting in Unconventional Oil Reservoirs With an Approximate Analytical Solution to the Double-Porosity Model. *SPE Reservoir Evaluation & Engineering* **2016**, *19*, 070–082. doi:10.2118/171031-pa.
23. Aybar, U.; Eshkalak, M.O.; Sepehrnoori, K.; Patzek, T.W. The effect of natural fractures closure on long-term gas production from unconventional resources. *Journal of Natural Gas Science and Engineering* **2014**, *21*, 1205–1213. doi:10.1016/j.jngse.2014.09.030.
24. Aybar, U.; Yu, W.; Eshkalak, M.O.; Sepehrnoori, K.; Patzek, T. Evaluation of production losses from unconventional shale reservoirs. *Journal of Natural Gas Science and Engineering* **2015**, *23*, 509–516. doi:10.1016/j.jngse.2015.02.030.

25. Patzek, T.W.; Male, F.; Marder, M. From the Cover: Gozzarelli Prize Winner: Gas production in the Barnett Shale obeys a simple scaling theory. *Proceedings of the National Academy of Sciences* **2013**, *110*, 19731–19736. doi:10.1073/pnas.1313380110.
26. Patzek, T.W.; Male, F.; Marder, M. A simple model of gas production from hydrofractured horizontal wells in shales. *AAPG Bulletin* **2014**, *98*, 2507–2529. doi:10.1306/03241412125.
27. Patzek, T.W.; Saputra, W.; Kirati, W. A Simple Physics-Based Model Predicts Oil Production from Thousands of Horizontal Wells in Shales. SPE Annual Technical Conference and Exhibition. Society of Petroleum Engineers, 2017. doi:10.2118/187226-ms.
28. Saputra, W.; Albinali, A.A. Validation of the Generalized Scaling Curve Method for EUR Prediction in Fractured Shale Oil Wells. SPE Kingdom of Saudi Arabia Annual Technical Symposium and Exhibition. Society of Petroleum Engineers, 2018. doi:10.2118/192152-ms.
29. Meissner, F.F. Petroleum geology of the Bakken Formation Williston Basin, North Dakota and Montana **1991**.
30. Sonnenberg, S.A.; Pramudito, A. Petroleum geology of the giant Elm Coulee field, Williston Basin. *AAPG Bulletin* **2009**, *93*, 1127–1153. doi:10.1306/05280909006.
31. LeFever, J.A. History of oil production from the Bakken Formation, North Dakota **1991**.
32. Nordeng, S. A brief history of oil production from the Bakken formation in the Williston Basin. *Geo News: North Dakota, Department of Mineral Resources Newsletter* **2010**.
33. Saputra, W.; Kirati, W.; Patzek, T. Generalized Extreme Value Statistics, Physical Scaling and Forecasts of Oil Production in the Bakken Shale. *Energies* **2019**, *12*, 3641. doi:10.3390/en12193641.
34. Patzek, T.; Saputra, W.; Kirati, W.; Marder, M. Generalized Extreme Value Statistics, Physical Scaling and Forecasts of Gas Production in the Barnett Shale. *Energy & Fuels* **2019**, *33*, 12154–12169. doi:10.1021/acs.energyfuels.9b01385.
35. Gumbel, E.J. *Statistics of Extremes*; Columbia University Press: New York, 1958.
36. Lantz, T.G.; Greene, D.T.; Eberhard, M.J.; Norrid, R.S.; Pershall, R.A. Refracture Treatments Proving Successful In Horizontal Bakken Wells. Rocky Mountain Oil & Gas Technology Symposium. Society of Petroleum Engineers, 2007. doi:10.2118/108117-ms.
37. Oruganti, Y.; Mittal, R.; McBurney, C.J.; Garza, A.R. Re-Fracturing in Eagle Ford and Bakken to Increase Reserves and Generate Incremental NPV: Field Study. SPE Hydraulic Fracturing Technology Conference. Society of Petroleum Engineers, 2015. doi:10.2118/173340-ms.
38. Ruhle, W. Refracturing: Empirical Results in the Bakken Formation. Proceedings of the 4th Unconventional Resources Technology Conference. American Association of Petroleum Geologists, 2016. doi:10.15530/urtec-2016-2461740.
39. Li, C.; Han, J.; LaFollette, R.; Kotov, S. Lessons Learned From Refractured Wells: Using Data to Develop an Engineered Approach to Rejuvenation. SPE Hydraulic Fracturing Technology Conference. Society of Petroleum Engineers, 2016. doi:10.2118/179148-ms.
40. Gullickson, G.; Ruhle, W.; Cook, P.F. The Lexicon of Recompletion: Empirical Justification for Refrac, Reentry, or Remediation in the Bakken/Three Forks Play. SPE Western Regional Meeting. Society of Petroleum Engineers, 2016. doi:10.2118/180414-ms.
41. Lane, W.; Chokshi, R. Considerations for Optimizing Artificial Lift in Unconventionals. Proceedings of the 2nd Unconventional Resources Technology Conference. American Association of Petroleum Geologists, 2014. doi:10.15530/urtec-2014-1921823.
42. Orji, E.; Lissanon, J.; Omole, O. Sucker Rod Lift System Optimization of an Unconventional Well. SPE North America Artificial Lift Conference and Exhibition. Society of Petroleum Engineers, 2016. doi:10.2118/181242-ms.
43. Oyewole, P. Artificial Lift Selection Strategy to Maximize Unconventional Oil and Gas Assets Value. SPE North America Artificial Lift Conference and Exhibition. Society of Petroleum Engineers, 2016. doi:10.2118/181233-ms.
44. Sickle, S.V.; Shelly, G.; Snyder, D. Optimizing Completions and Artificial Lift in an Unconventional Play in the United States. SPE Artificial Lift Conference — Latin America and Caribbean. Society of Petroleum Engineers, 2015. doi:10.2118/173974-ms.

45. Eftekhari, B.; Marder, M.; Patzek, T.W. Field data provide estimates of effective permeability, fracture spacing, well drainage area and incremental production in gas shales. *Journal of Natural Gas Science and Engineering* **2018**, *56*, 141–151. doi:10.1016/j.jngse.2018.05.027.
46. Male, F.; Marder, M.; Browning, J.; Gherabati, A.; Ikonnikova, S. Production Decline Analysis in the Eagle Ford. Proceedings of the 4th Unconventional Resources Technology Conference. American Association of Petroleum Geologists, 2016. doi:10.15530/urtec-2016-2458308.
47. Male, F.; Gherabati, A.; Browning, J.R.; Marder, M. Forecasting Production From Bakken and Three Forks Wells Using a Segregated Flow Model. Proceedings of the 5th Unconventional Resources Technology Conference. American Association of Petroleum Geologists, 2017. doi:10.15530/urtec-2017-2666809.
48. Kondash, A.J.; Albright, E.; Vengosh, A. Quantity of flowback and produced waters from unconventional oil and gas exploration. *Science of The Total Environment* **2017**, *574*, 314–321. doi:10.1016/j.scitotenv.2016.09.069.
49. Cheng, Y. Impact of Water Dynamics in Fractures on the Performance of Hydraulically Fractured Wells in Gas-Shale Reservoirs. *Journal of Canadian Petroleum Technology* **2012**, *51*, 143–151. doi:10.2118/127863-pa.
50. Abualfaraj, N.; Gurian, P.L.; Olson, M.S. Characterization of Marcellus Shale Flowback Water. *Environmental Engineering Science* **2014**, *31*, 514–524. doi:10.1089/ees.2014.0001.
51. Hughes, J.D. 2016 Tight Oil Reality Check. *Post Carbon Institude: Santa Rosa, CA, USA* **2016**.
52. Hughes, J.D. Shale Reality Check. *Post Carbon Institude: Santa Rosa, CA, USA* **2018**.
53. Hughes, J.D. How Long Will the Shale Revolution Last?: Technology versus Geology and the Lifecycle of Shale Plays. *Post Carbon Institude: Santa Rosa, CA, USA* **2019**.
54. Paneitz, J. Evolution of the Bakken Completions in Sanish Field, Williston Basin, North Dakota. *SPE ATW: Maximizing Tight Oil in the Bakken Keystone, Colorado. PowerPoint Presentation. August* **2010**, *6*.
55. Buffington, N.; Kellner, J.; King, J.G.; David, B.L.; Demarchos, A.S.; Shepard, L.R. New Technology in the Bakken Play Increases the Number of Stages in Packer/Sleeve Completions. SPE Western Regional Meeting. Society of Petroleum Engineers, 2010. doi:10.2118/133540-ms.
56. Weddle, P.; Griffin, L.; Pearson, C.M. Mining the Bakken: Driving Cluster Efficiency Higher Using Particulate Diverters. SPE Hydraulic Fracturing Technology Conference and Exhibition. Society of Petroleum Engineers, 2017. doi:10.2118/184828-ms.
57. Martin, E. *United States Tight Oil Production 2018*, 2009 (accessed March 25, 2019).
58. Jin, H.; Sonnenberg, S.A. Characterization for Source Rock Potential of the Bakken Shales in the Williston Basin, North Dakota and Montana. Unconventional Resources Technology Conference, Denver, Colorado, 12-14 August 2013. Society of Exploration Geophysicists, American Association of Petroleum Geologists, Society of Petroleum Engineers, 2013. doi:10.1190/urtec2013-013.
59. Han, Y.; Misra, S.; Simpson, G.; others. Dielectric dispersion log interpretation in Bakken petroleum system. SPWLA 58th Annual Logging Symposium. Society of Petrophysicists and Well-Log Analysts, 2017.
60. Han, Y.; Misra, S. Bakken Petroleum System Characterization Using Dielectric-Dispersion Logs. *Petrophysics - The SPWLA Journal of Formation Evaluation and Reservoir Description* **2018**, *59*, 201–217. doi:10.30632/pjv59n2-2018a6.
61. Alvarez, D.; Joseph, A.; Gulewicz, D. Optimizing Well Completions in the Canadian Bakken: Case History of Different Techniques to Achieve Full ID Wellbores. SPE Unconventional Resources Conference Canada. Society of Petroleum Engineers, 2013. doi:10.2118/167148-ms.
62. Kurtoglu, B. *Integrated reservoir characterization and modeling in support of enhanced oil recovery for Bakken*; Colorado School of Mines, 2013.
63. Tran, T.; Sinurat, P.D.; Wattenbarger, B.A. Production Characteristics of the Bakken Shale Oil. SPE Annual Technical Conference and Exhibition. Society of Petroleum Engineers, 2011. doi:10.2118/145684-ms.

 doi:10.20944/preprints201912.0334.v1

Appendix A Bakken reservoir properties, summary of matching parameters, and details of EURs

Table A1. Reservoir properties used in scaling oil production in the Middle Bakken and Upper Three Forks

Parameter	Middle Bakken		Upper Three Forks		Data source
	SI units	Field units	SI units	Field units	
Horizontal well length, L_w	2900 m	9500 ft	2900 m	9500 ft	DrillingInfo
Number of fracture stages, N	30	30	30	30	DrillingInfo
Fracture height, H	10 m	33 ft	12 m	40 ft	well log
Tip-to-tip fracture length, $2L$	360 m	1200 ft	360 m	1200 ft	DrillingInfo
Reservoir temperature, T	113°C	237°F	115°C	239°F	[62]
Initial pressure, p_i	36.8 Mpa	5340 psia	37.1 Mpa	5380 psia	well log
Saturation pressure, p_b	17.4 Mpa	2530 psia	12.1 Mpa	1753 psia	[62]
Fracture pressure, p_f	3.4 Mpa	500 psia	3.4 Mpa	500 psia	DrillingInfo
Connate water saturation, S_{wc}	0.57	0.57	0.65	0.65	well log
Initial oil saturation, S_{oi}	0.43	0.43	0.35	0.35	well log
Rock porosity, ϕ	0.046	0.046	0.058	0.058	well log
Rock permeability, k	4.4×10^{-17} m^2	0.045 md	4.6×10^{-17} m^2	0.047 md	well log
Rock compressibility, c_ϕ	4.3×10^{-10} Pa^{-1}	3.0 microsip	4.3×10^{-10} Pa^{-1}	3 microsip	[63]
Water compressibility, c_w	4.3×10^{-10} Pa^{-1}	3 microsip	4.3×10^{-10} Pa^{-1}	3 microsip	[63]
Oil compressibility, c_o	1.4×10^{-9} Pa^{-1}	1 microsip	1.4×10^{-9} Pa^{-1}	1 microsip	[63]
Oil viscosity, μ_{oi}	3.9×10^{-5} Pa s	0.392 cp	2.8×10^{-5} Pa s	0.276 cp	[62]
Oil formation volume factor, B_{oi}	1.61 m^3/sm^3	1.61 rbbl/stb	1.48 m^3/sm^3	1.48 rbbl/stb	[62]
API gravity	42°API	42°API	39°API	39°API	[62]
GOR	1.48 sm^3/sm^3	125 scf/stb	110 sm^3/sm^3	620 scf/stb	[62]

Table A2. Summary of pressure interference time, τ, and mass of oil in place, $\mathcal{M}$, for four different well classes in the Middle Bakken and Upper Three Forks

Well class	Middle Bakken							Upper Three Forks						
	τ (months)			$\mathcal{M}$ (ktons)			number	τ (months)			$\mathcal{M}$ (ktons)			number
	P_{10}	P_{50}	P_{90}	P_{10}	P_{50}	P_{90}	of wells	P_{10}	P_{50}	P_{90}	P_{10}	P_{50}	P_{90}	of wells
Interfering	170	100	50	720	420	190	4245	140	90	40	540	320	150	2156
Non-Interfering	250	220	180	860	480	250	3349	250	210	160	680	400	170	1496
Refracs	230	150	70	1210	660	230	1549	230	140	70	980	540	200	814
Newly completed	60	50	30	800	520	270	751	60	40	30	620	400	200	528
All wells	200	150	90	850	490	220	9894	180	130	80	660	390	170	4994

Table A3. Bakken EUR Summary

AU	State	County	EIA 2019				Physical Scaling							
			Bakken		Three Forks		Bakken				Three Forks			
			EUR	Potential	EUR	Potential	P10	P50	P90	Existing	P10	P50	P90	Existing
			(Mb/well)	wells	(Mb/well)	wells	(Mb/well)	(Mb/well)	(Mb/well)	wells	(Mb/well)	(Mb/well)	(Mb/well)	wells
Central Basin	MT	Daniels	60	189			-	-	-	-	-	-	-	-
Central Basin	MT	McCone	60	528			196	196	196	1	-	-	-	-
Central Basin	MT	Richland	232	1083			318	210	103	102	234	118	44	3
Central Basin	MT	Roosevelt	263	4985			330	212	103	138	228	129	38	11
Central Basin	MT	Sheridan	49	753			359	163	37	4	64	59	53	2
Central Basin	ND	Divide	241	12			-	-	-	-	99	-307	27	3
Central Basin	ND	Dunn	184	73			459	301	156	41	375	254	160	14
Central Basin	ND	McKenzie	263	3749			465	298	158	1540	399	250	125	669
Central Basin	ND	Williams	262	3070			463	300	162	1261	376	250	143	524
Eastern Transitional	ND	Burke	7	2706			267	153	62	117	235	148	81	24
Eastern Transitional	ND	Divide	140	658			237	140	64	96	311	182	78	206
Eastern Transitional	ND	Dunn	423	1099			620	354	125	248	554	335	208	111
Eastern Transitional	ND	Hettinger	169	7			-	-	-	-	-	-	-	-
Eastern Transitional	ND	McLean	623	245			523	310	144	40	1198	501	193	4
Eastern Transitional	ND	Mercer	13	144			-	-	-	-	-	-	-	-
Eastern Transitional	ND	Mountrail	232	2679			683	388	155	1163	464	274	114	201
Eastern Transitional	ND	Stark	169	371			177	177	177	1	125	21	11	2
Eastern Transitional	ND	Ward	80	111			209	209	209	1	-	-	-	-
Elm Coulee - Billings Nose	MT	McCone	80	116			-	-	-	-	-	-	-	-
Elm Coulee - Billings Nose	MT	Richland	183	3421			423	230	75	935	112	64	15	2
Elm Coulee - Billings Nose	ND	Billings	60	828	177	35870	263	192	17	10	265	149	59	37
Elm Coulee - Billings Nose	ND	Golden Valley	476	130			70	70	70	1	502	337	172	12
Elm Coulee - Billings Nose	ND	McKenzie	184	2449			269	157	62	79	291	134	9	8
Nesson - Little Knife	ND	Billings	167	586			268	135	31	49	280	165	76	82
Nesson - Little Knife	ND	Burke	188	680			258	174	95	65	265	173	91	68
Nesson - Little Knife	ND	Divide	115	603			246	159	82	128	236	151	77	149
Nesson - Little Knife	ND	Dunn	324	2685			615	358	185	1258	569	345	181	608
Nesson - Little Knife	ND	Hettinger	223	106			-	-	-	-	-	-	-	-
Nesson - Little Knife	ND	McKenzie	329	1520			651	397	200	1072	610	362	164	1006
Nesson - Little Knife	ND	Mountrail	312	530			545	326	147	975	503	304	146	655
Nesson - Little Knife	ND	Slope	120	167			-	-	-	-	-	-	-	-
Nesson - Little Knife	ND	Stark	156	2164			199	167	134	2	343	203	93	219
Nesson - Little Knife	ND	Williams	178	1828			365	213	96	410	349	211	100	243
Northwest - Transitional	MT	Daniels	82	2584			-	-	-	-	-	-	-	-
Northwest - Transitional	MT	McCone	82	161			-	-	-	-	-	-	-	-
Northwest - Transitional	MT	Roosevelt	82	1312			-	-	-	-	-	-	-	-
Northwest - Transitional	MT	Sheridan	50	2857			195	100	24	27	67	67	67	1
Northwest - Transitional	MT	Valley	1	1005			-	-	-	-	-	-	-	-
Northwest - Transitional	ND	Divide	180	601			248	158	87	41	239	153	77	110
Northwest - Transitional	ND	Williams	212	669			311	185	81	89	317	224	85	20
AVERAGE EUR (thousand bbl)			189		177		515	309	146		456	278	136	
TOTAL WELL				49464		35870				9894				4994
TOTAL EUR (billion bbl)			9.3		6.3		5.1	3.1	1.4		2.3	1.4	0.7	

doi:10.20944/preprints201912.0334.v1